Hourly composition of gas and particle phase pollutants at a central urban background site in Milan, Italy

A. Bigi[a], F Bianchi[b,c], G. De Gennaro[d], A. Di Gilio[d,h], P. Fermo[e], G. Ghermandi[a], A. S. H. Prévôt[b], M. Urbani[e,i], G. Valli[f], R. Vecchi[f], A. Piazzalunga[g,j]

[a]*Department of Engineering "Enzo Ferrari", Università degli studi di Modena e Reggio Emilia, Modena, Italy*
[b]*Laboratory of Atmospheric Chemistry, Paul Scherrer Institute, Villigen, Switzerland*
[c]*Department of Physics, University of Helsinki, Helsinki, Finland*
[d]*Department of Chemistry, Università degli studi di Bari, Bari, Italy*
[e]*Department of Chemistry, Università degli studi di Milano, Milan, Italy*
[f]*Department of Physics, Università degli studi di Milano, Milan, Italy*
[g]*Department of Environmental Sciences, Università degli studi di Milano Bicocca, Milan, Italy*
[h]*Now at ARPA Puglia, Bari, Italy*
[i]*Now at Chemservice Controlli e Ricerche s.r.l., Novate Milanese, Italy*
[j]*Now at Water and Life Lab, Entratico, Italy*

Abstract

A comprehensive range of gas and particle phase pollutants were sampled at 1–hour time resolution in urban background Milan during summer 2012. Measurements include several soluble inorganic aerosols (Cl^-, NO_2^-, NO_3^-, SO_4^{2-}, Ca^{2+}, K^+, Mg^{2+}, Na^+, NH_4^+) and gases (HCl, HNO_2, HNO_3, NH_3, NO, NO_2, O_3, SO_2), organic, elemental and black carbon and meteorological parameters. Analysis methods used include mean diurnal pattern on weekdays and Sundays, pollution roses, bivariate polar plots and statistical models using backtrajectories. Results show how nitrous acid (HONO) was mainly formed heterogeneously at nighttime, with a dependence of its

Email address: pzzndr77@gmail.com (A. Piazzalunga)

formation rate on NO_2 consistent with observations during the last HONO campaign in Milan in summer 1998, although since 1998 a drop in HONO levels occurred following to the decrease of its precursors. Nitrate showed two main formation mechanisms: one occurring through N_2O_5 at nighttime and leading to nitrate formation onto existing particles; another occurring both daytime and nighttime following the homogeneous reaction of ammonia gas with nitric acid gas. Air masses reaching Milan influenced nitrate formation depending on their content in ammonia and the timing of arrival. Notwithstanding the low level of SO_2 in Milan, its peaks were associated to point source emissions in the Po valley or shipping and power plant emissions SW of Milan, beyond the Apennines. A distinctive pattern for HCl was observed, featured by an afternoon peak and a morning minimum, and best correlated to atmospheric temperature, although it was not possible to identify any specific source. The ratio of primary-dominated organic carbon and elemental carbon on hourly $PM_{2.5}$ resulted 1.7. Black carbon was highly correlated to elemental carbon and the average mass absorption coefficient resulted MAC $= 13.8 \pm 0.2\,m^2g^{-1}$. It is noteworthy how air quality for a large metropolitan area, in a confined valley and under enduring atmospheric stability, is nonetheless influenced by sources within and outside the valley.

Keywords: $PM_{2.5}$, hourly ionic composition, gas-phase pollutants, Po valley

---

1. Introduction

The interactions between gaseous and aerosol phase pollutants have long been studied due to their impact on air quality (Penkett et al., 1979; Rav-

ishankara, 1997) and on human health (World Health Organization, 2006). In order to investigate processes leading to atmospheric pollutants formation and ageing in densely populated areas with large emission load (i.e. hotspots), time resolved composition of both gas and particle phase atmospheric compounds are needed. Po valley (Northern Italy) is one of the most important hotspot region in Europe (Putaud et al., 2010), with Milan metropolitan area exhibiting one of the poorest air quality within the valley (Bigi and Ghermandi, 2014).

Very few 1-hour time resolution campaigns were accomplished in Milan urban area. Three noteworthy studies resulted from the Limitation of Oxidant Production/Pianura Padana Produzione di Ozono (LOOP/PIPAPO) campaign held in May and June 1998 in Milan urban background (Neftel et al., 2002). In one of these studies Baltensperger et al. (2002) analysed data by several continuous instruments sampling aerosol physical properties (number size distribution, volatility, hygroscopicity, mass), aerosol chemical composition (BC_E, nitrate, sulphate) and two gases (NH_3, HNO_3). This same study showed the large contribution to airborne particles smaller than 40 nm by primary emissions rich in soot content and the increase in secondary and hygroscopic aerosol for particles larger than 50 nm. The second study within PIPAPO, Putaud et al. (2002) collected samples of size-segregated aerosol with 4– and 7–hour time resolution and analysed them for elemental carbon (EC), organic carbon (OC), particulate organic matter (POM) and major ionic species; their results showed the large contribution ($> 30\%$) to

PM mass by POM, by ammonium nitrate (29% of PM mass) and ammonium sulphate (22% of PM mass). Putaud et al. (2002) found also a diurnal and weekly pattern for traffic-related pollutants (e.g. EC and resuspended mineral dust), the influence of traffic emissions on nitrate formation and of industrial emissions on sulphate formation. In the third study of PIPAPO Alicke et al. (2002) investigated hydroxyl radical formation by measuring several gas phase pollutants by DOAS (Differential Optical Absorption Spectroscopy): HCHO, HONO, NO_2, NO, O_3 and SO_2. Their results identified HCHO as the primary source of $OH^{\cdot}$ radicals (up to 40% of total $OH^{\cdot}$ on clear days), while photolysis of nitrous acid and of ozone provides similar contribution to atmospheric $OH^{\cdot}$ (15–30% of total $OH^{\cdot}$ each), with the former compound dominating during early morning and the latter during the afternoon. In addition to the above mentioned studies, the aerosol elemental composition and sources were investigated with hourly resolution in Milan by D'Alessandro et al. (2003, 2004) during wintertime and summertime 2001 evidencing quasi-periodical and episodic pollution sources.

Several sources influence the sampling site: Bernardoni et al. (2011) used Positive Matrix Factorization to apportion 4–hour PM_{10} measurements and showed the diurnal pattern in the relative contribution by resuspended dust, construction works and industry, which altogether account for 48% to total PM_{10} in summer. These results were confirmed by the a detailed source apportionment exercise in Milan urban background by Perrone et al. (2012), where three years of daily $PM_{2.5}$ and PM_{10} samples were analysed. This

latter study also showed how 60% of summer daily $PM_{2.5}$ derives from traffic and secondary inorganic ions (sulphate, nitrate and ammonium) and contribution of resuspended dust to summer daily $PM_{2.5}$ is only to 3.8%. Consistently emission inventory for the only municipality of Milan assessed Road Traffic (SNAP 7) to be the main source of NO_x and EC for the city of Milan, SNAP 2 (non–industrial combustion) is the main source of OC and the second most important of NO_x, and SNAP 6 (solvent use) is the main source of $NM-VOC$. Notwithstanding these studies, in Milan there is no available analysis of simultaneous characterization of atmospheric pollutants in both gas and particle phase sampled at a 1-hour resolution. The present article is based on a thorough analysis of measurements of several gas phase pollutants and main chemical composition of $PM_{2.5}$ sampled at 1–hour time resolution. Formation process of $PM_{2.5}$ in Milan will be presented along with the influence of meteorological conditions and air mass trajectories. Observations include HCl, HONO, HNO_3 and NH_3, i.e. the first published measurement of hydrochloric acid in the Po valley and the first 1-hour resolution measurements of nitrous and nitric acids in the last 15 years in Milan. Details on the instrumentation and methods used are presented in Sect. 2. Results and conclusions are found in Sects. 3 and 4 respectively.

2. Data and methods

Milan (45 °28'N; 9 °13'E) urban area counts about 1 500 000 inhabitants and is the second largest town in Italy, after Rome, and considering the whole

Milan province the population rises up to about 3.1 millions inhabitants.

The data here presented were collected on the roof of the Department of Chemistry, University of Milan, at a ∼10 m a.g.l. within the University campus, a site representative of central urban background conditions for the city. Sampling was performed from June 5th until July 23rd 2012.

Hourly resolution composition of $PM_{2.5}$ for soluble inorganic ions composition and for gases was determined using a commercially available Ambient Ion Monitor (AIM) URG–9000D (URG Corp, USA). In particle phase five anions (Cl^-, F^-, NO_2^-, NO_3^-, SO_4^{2-}) and five cations (Ca^{2+}, K^+, Mg^{2+}, Na^+, NH_4^+) were determined. F^-, Ca^{2+}, K^+, Mg^{2+} and Na^+ were often below the detection limit and therefore not analysed in details. The gases determined include hydrochloric acid (HCl), nitrous acid (HONO), nitric acid (HNO_3), ammonia (NH_3) and sulphur dioxide (SO_2). The AIM consists of a sampling system for both gas and particles, coupled with two ion chromatographies for the analytical determination. Gases are collected by a liquid diffusion denuder with H_2O_2 5 mM running continuously at 10 mL h^{-1} flow rate. Particles are collected in a chamber supersaturated with ultrapure water vapour: water soluble particles are allowed to grow and then inertially separated and injected into the ion chromatographies. Further instrumental details and the calibration procedure used in this study can be found in Markovic et al. (2012). AIM data were compared to off-line daily data from $PM_{2.5}$ samples collected during 22 days throughout the campaign by denuded filter-pack setup (Vecchi et al., 2009): the system consisted in two dry annular denud-

ers removing both acidic and basic gases, followed by a filter pack made of a quartz fibre front filter and a nylon fibre backup filter. Once the campaign ended, AIM blank values for particle-phase aerosol were estimated by inserting a quartz fibre filter between the denuder and the filter pack over 5 full days.

Comparison of AIM and denuded filter pack showed statistically significant (by ANOVA test) and large coefficients of determination for linear regression models between off– and on–line data for all species (Figure S1), supporting the reliability of the patterns observed by AIM. Regression coefficients were close to unity for HNO_2+HNO_3 and NH_3, while some difference occurred between particle-phases compounds, with lower NO_2^-+NO_3^- levels observed by AIM and lower values for SO_4^{2-} and NH_4^+ observed by denuded filter-pack. Assuming that the denuded filter pack reported in Vecchi et al. (2009) is artefact-free for nitrogen compounds, some bias likely affects ammonium in AIM measurements, preventing a fully–correct estimate of ion balance for the experimental dataset. Part of the offset between the two measurement sets might also be due to the possibly different transmission efficiency curve between respective size-selective inlets: AIM uses a custom $PM_{2.5}$ cyclone, while denuded filter pack used a US-EPA equivalent $PM_{2.5}$ inlet equipped with a PM_{10} sampling head and a WINS $PM_{2.5}$ impactor downstream.

Gaseous precursors levels during AIM blank test resulted similar to their respective mean observed during the campaign, indicating an efficient collection of gas and a complete transmission of particles by the denuders. Significant

particulate sodium was observed during blanks and ascribed to contamination in the ultrapure water used in the supersaturated chamber during the blank test. The low particulate nitrite, nitrate and ammonium observed during blank testing (i.e. $< 1\,\mu g\,m^{-3}$) can be considered negligible. Slightly larger blank for particulate sulphate was observed ($\sim 1.5\,\mu g\,m^{-3}$), but considered sufficiently low to support the reliability of the AIM measurements for this compound.

Elemental carbon (EC) and organic carbon (OC) measurements were collected by a Model-4 Semi-Continuous ECOC Field Analyser by Sunset Laboratory, USA (Bae et al., 2004). The carbon analyser was provided with a $PM_{2.5}$ cyclone and operated at a $24\,L\,min^{-1}$ flowrate. Measurement had 1–hour time resolution, comprising 45 minutes for sampling and 15 minutes for thermal-optical analysis. The analysis followed a high temperature analytical protocol featured by 2 steps in inert atmosphere (625 °C, 870 °C) and 3 steps in oxidizing atmosphere (650 °C, 675 °C, 870 °C). During most of the campaign the split point (i.e. the separation between OC and EC) occurred in inert atmosphere: the pre-combustion of EC was attributed to the low carbon amount and to the presence of undesired oxygen or of metal oxides accumulated on the filter. The data analysis included only EC–OC measurement having a split point above 650 °C (Jung et al., 2011), in accordance with EUSAAR2 protocol for off-line laboratory measurements (Cavalli et al., 2010). Both calibration and filter replacement were performed on a weekly basis; no EC–OC data are available on Sundays.

Aerosol light absorption coefficient (σ_{ap}) was measured by a Multi-Angle Absorption Photometer (MAAP, model 5012, Thermo Scientific Corp., USA) equipped with a $PM_{2.5}$ inlet. Atmospheric equivalent black carbon concentration (BC_E) is estimated by the instrument using a MAC (mass specific absorption cross section) of $6.6\,m^2\,g^{-1}$ (Petzold et al., 2002). BC_E measurements had a 5-min resolution and the data were then averaged to 1 hour. To evaluate atmospheric dispersion conditions, ^{222}Rn short-lived decay products measurements were performed using the experimental methodology reported in Marcazzan et al. (2003). Hourly measurements of meteorological parameters (wind speed and direction, temperature, relative humidity, pressure, global solar radiation and precipitation) were sampled on the roof of the Department of Physics, University of Milan, at ∼10 m a.g.l., within the grounds of the University campus. Concentration of NO, NO_2 and O_3 were provided by an urban background station sited 400 m NE of the campus and within the air quality monitoring network of the Regional Environmental Protection Agency of Lombardy (ARPA).

A tentative localization and identification of the pollution sources was performed by four techniques: analysis of conditional bivariate probability function (CBPF), bivariate polar plots, air mass origin by simulated backtrajectory and backtrajectory statistical models (BSMs). The former two techniques are headed to identify local sources, while backtrajectories were used to potentially track pollution events due to distant sources. CBPF

technique estimates the probability that a specific concentration range is observed within a given wind sector, depending upon wind speed (more details in Uria-Tellaetxe and Carslaw, 2014). Bivariate polar plots (Carslaw and Ropkins, 2012) are a level plot in polar coordinates where colour scale represents pollutant concentration and polar coordinates are a smoothed interpolation of wind speed and wind direction by Generalised Additive Model (Wood, 2006). Origin of air masses arriving in Milan at 100 m a.g.l. was estimated with 36–hours long backtrajectories simulated by HYSPLIT (Draxler and Rolph, 2013) using 0.5° GDAS meteorological data. 24 trajectories per day were computed, i.e. one per hour. The statistical models applied to backtrajectories include Concentration Field (CF), Potential Source Contribution Function (PSCF) and Gridded Difference (GD) using respective functions in Carslaw and Ropkins (2012). All of the three attempt to combine trajectory path to concentration at the receptor; further details about BSMs can be found in Carslaw and Ropkins (2012) and Fleming et al. (2012). Scheifinger and Kaiser (2007) proved BSMs to provide useful information on potential source areas only for distances within the mean residence time of the investigated compound; for trajectories longer than this period the effect of turbulent dispersion and removal processes, neglected by the statistical models and the backtrajectories, may lead to unreliable results (Han et al., 2005). In the present study trajectory statistical models were tested for several species, although significant results occurred only for SO_2, SO_4^{2-} and NH_3. For sulphur dioxide Scheifinger and Kaiser (2007) suggest to limit backtrajectories

within 60 hours: in this study a length of 36 hours (i.e. largely within 60 hours) was used for all pollutants.

Few different emission inventories were used to review BSM outputs and to identify realistic potential sources: a plot pairing inventory database and corresponding area is presented in Figure S2. Emission inventories for Lombardy, Piedmont and Veneto were consistently compiled (INEMAR, 2015), resulting in a bottom-up inventory with a spatial resolution at the municipality district level. These inventories are compliant to the EMEP–CORINAIR guidebook, the IPCC guidelines and the Good Practice Guidance, they are classified accordingly to SNAP (Selected Nomenclature for Air Pollution) and the emission data used in this study refers to 2010 for Lombardy and 2008 for Piedmont and Veneto. Emissions for Aosta Valley, Liguria, Rhône Alpes and Provence–Alpes–Côte d'Azur refers to 2008, have a spatial resolution at the municipality district level and include point sources for the three former regions. Data were provided by the project AERA (Air Environnement Regions ALCOTRA) through a Web Map Service (AERA, 2015). Finally, emissions for all other regions involved in this study were provided by the UNECE/EMEP emission inventory for 2012. Accuracy and uncertainty of these inventories are different, as well as the procedure to build them, their spatial resolution and their reference year. In this study inventories were used to identify areas with significant SO_2 emissions (e.g. large industrial plants) and to approximately compare potential sources, therefore

the discrepancies between these databases were considered negligible for the purpose of this analysis. Nonetheless the closer the investigated area is to Milan, the more detailed is the inventory used, allowing a reliable analysis of nearby and directly impacting sources.

All statistical data analyses were performed within the software environment R 3.0.2 (R Core Team, 2013). All data are reported in local time, i.e. Central European Summer Time (CEST).

3. Results and discussion

In the following the data will be presented and discussed in specific subsections for each common species, including their pattern, formation and removal processes (if known) and their potential source. The analysis investigates the average concentration pattern over the whole sampling period, and the variability of a subset of pollutants under different atmospheric dispersion conditions.

3.1. Meteorological setting

June and July 2012 were featured by high pressure fields originated by the Azores high and occasionally by subtropical anticyclones (Figure S3). Large values of mean geopotential height at 500 hPa occurred during the sampling campaign, when June was characterized by anticyclonic curvature and moderately positive anomaly and July by a slightly cyclonic curvature. This meteorological context determined recurrent atmospheric stability, clear-sky

and high temperatures, enhancing photochemical activity and formation of tropospheric ozone. Hot weather conditions occurred between the end of June and the beginning of July and, after a short instability period, since July 8^{th}. Main meteorological events reducing atmospheric pollutants levels occurred at the beginning of June prompted by moderately perturbed fluxes and Atlantic cold fronts, on the 14^{th} and 15^{th} of July due to ventilation originated by a temporary positioning in the North of Alps of the maximum of the Azores high, and on July 21^{st} when a cold front led to intense rainstorms in Milan and surroundings. A mountain-valley breeze regime was present during large part of the campaign, with low N winds at night ($< 2\,\mathrm{m\,s^{-1}}$), increasing and rotating at daytime until a SW flow is established in the afternoon with speeds up to $4\,\mathrm{m\,s^{-1}}$. These meteorological conditions were typical of summers in Northern Italy, therefore notwithstanding measurements did not cover the whole summer, they are well representative of the entire season. A summary of statistical values for the measured parameters is presented in table B.1. In Figure B.1 the diurnal pattern during weekdays and Sundays are presented for several observed pollutants, along with temperature (T), Radon concentration (Rn), global radiation (GR) and relative humidity (RH).

3.2. Nitrogen oxides and ozone

Nitric oxide shows sharp peaks at mornings only on weekdays, indicating a source from rush hour traffic, along with relatively low atmospheric mixing;

NO rapidly declines due to vertical mixing and its oxidation to NO_2 by O_3 and by the available radical groups.

Nitrogen dioxide peaks at morning rush hours. The afternoon decrease in NO_2 is driven by 3 processes: dilution due to the rise in mixing layer height, photolysis to NO under intense solar radiation and reaction with $OH^{\cdot}$ to nitric acid. The difference between weekdays and Sundays is noteworthy for both NO and NO_2, strongly indicating an anthropogenic source, most likely traffic, of these compounds.

Ozone shows an afternoon peak generated by the large availability of $OH^{\cdot}$ radicals and possibly by the re-entrainment of O_3 within the residual layer (Zhang and Trivikrama Rao, 1999). Indeed the sum of NO_2 and O_3 shows a slightly higher peak on weekdays indicating the small contribution by fresh emissions to oxidant species. Ozone exhibits a very mild weekend effect (Cleveland et al., 1974; Jiménez et al., 2005; Tonse et al., 2008; Pollack et al., 2012; Wang et al., 2014), e.g. higher mixing ratios on Sundays due to lower NO_x emissions over the weekend and therefore reduced titration of O_3, as shown for Milan by Vecchi and Valli (1999). Since 1700 CEST mixing decreases leading to an increase in NO_x and a drop in ozone. Diurnal pattern for NO_x and O_3 are highly similar to mean diurnal pattern for long term measurements in Modena, 160 km SE of Milan, Po valley (Bigi et al., 2012), where ozone exhibits also similar levels to those observed in Milan, consistently with the atmospheric homogeneity across the valley.

3.3. Nitrous acid and nitrites

Gas-phase nitrous acid (HONO) shows a pattern similar to past observations in Milan by Stutz et al. (2002) and Febo et al. (1996), featured by lower mixing ratios at daytime, due to photolysis, and peak at nighttime, most likely by heterogeneous formation. Particle-phase nitrites (NO_2^-) exhibit a diurnal pattern highly similar to HONO, as observed in Marseille (Acker et al., 2005), suggesting that part of atmospheric HONO is formed heterogeneously onto particle surfaces under high RH conditions. Traffic emissions are another possible source of HONO: Kurtenbach et al. (2001) found large variability in the ratio $HONO/NO_x$ from road tunnel measurements depending on fuel, emission control systems and motor load. A ratio for $HONO/NO_x$ of 1 % was used in this study, similarly to the ratio used by Michoud et al. (2014) for Paris and higher than 0.65 % as used by Stutz et al. (2002) for Milan. In order to remove HONO direct emissions from total HONO, secondary HONO was estimated as $HONO_{sec} = HONO - 0.01 \cdot NO_x$, resulting in a ~ 80 % of total HONO from secondary origin.

Main formation mechanism of $HONO_{sec}$ in urban atmosphere is expected to proceed heterogeneously onto surfaces, following reactions 1 and 2, with 1 being the most likely process (Kleffmann, 2007). It is still unclear whether the contribution of heterogeneous formation of $HONO_{sec}$ onto soot particles (Kalberer et al., 1999) is a significant source to atmospheric concentrations (Kleffmann, 2007; Ziemba et al., 2010) or not (Finlayson-Pitts and Pitts,

2000).

$$2NO_2 + H_2O \rightarrow HONO_{sec} + HNO_{3(ads)} \quad (1)$$

$$NO_2 + NO + H_2O \rightarrow 2HONO_{sec} \quad (2)$$

Latest published measurements of nitrous acid in Milan urban background were collected in May and June 1998 by Alicke et al. (2002) and Stutz et al. (2002). The latter investigated HONO formation by DOAS–resolved vertical profiles and found that $HONO_{sec}$ was formed at ground. Stutz et al. (2002) estimated that 1 molecule of $HONO_{sec}$ was released each 25–40 molecules of NO_2 and assessed the NO_2 conversion efficiency to be an order of magnitude lower than expected according to reaction 1.

In Alicke et al. (2002) HONO mixing ratios by DOAS exhibited a nighttime and daytime mean of 0.92 ppb and 0.14 ppb respectively. In summer 2012 the mean mixing ratios observed were of 0.6 ppb at nighttime and 0.5 ppb at daytime, with the latter being largely higher than in 1998 and potentially biased by artefacts. Maximum nitrous acid levels were similar in both studies: 4.4 ppb and 4.2 ppb in 1998 and 2012 respectively.

In order to assess whether a long term trend in HONO is present and 2012 daytime data are artefact-freefall, an analysis of NO_2 levels from 1998 through 2012 was performed. Mean daytime NO_2 concentration during the two sampling campaigns were 18.3 ppb and 4.9 ppb in 1998 and 2012 respectively, while mean nighttime NO_2 concentration was 33.2 ppb in 1998 and 8.8 ppb in 2012. These observations are consistent with an estimated

long term trends for deseasonalized monthly mean concentration of NO_2 of -1.47 ± 0.17 ppb yr^{-1} (trends are estimated by Generalised Least Squares method as in Bigi and Ghermandi (2014)). Given the large NO_2 concentrations in 1998, Stutz et al. (2002) found a large contribution of direct emissions to atmospheric HONO, notwithstanding they made use of a low $HONO/NO_x$ ratio, i.e. 0.65%. The large decrease in NO_2 from 1998 to 2012 should cause a significant decrease in HONO over the same period, although, according to 2012 HONO data, a decrease occurred only at nighttime. Several intercomparison studies of HONO measurements by DOAS and chemical instruments (e.g. wet denuder and LOPAP) showed how results from different techniques agreed well at nighttime, while HONO by standard wet denuders might suffer from positive artefacts at daytime (Kleffmann et al., 2006): these might occur by reaction on denuder surface either of semivolatile diesel exhausts with NO_2 (Gutzwiller et al., 2002), either of pure NO_2 (Kleffmann et al., 2006), either of NO_2 and S(IV) (Spindler et al., 2003). The high HONO and $HONO_{sec}/NO_2$ ratio in 2012 at daytime suggest that 2012 daytime HONO mixing ratios might be biased by a chemical interference in the denuder, since are not consistent with the observed decrease in NO_2 from 1998 to 2012 and the corresponding decrease in nighttime HONO over the same period.

Assuming that during nighttime most of nitrous acid is formed through reaction 1, which is first order in NO_2, formation rate between two generic

instants t_1 and t_2 was computed according to equation 3.

$$\overline{F_{HONO_{sec}}} = \frac{[HONO_{sec}](t_2) - [HONO_{sec}](t_1)}{(t_2 - t_1)[NO_2]_{night}} \quad (3)$$

Formation rate is best estimated for nights when NO and NO_2 levels are low, in order to consider negligible both direct HONO emissions by traffic and positive artefacts, and when HONO formation is steady and lasts throughout the night, in order to average over several hours. These conditions are met between June 18^{th}–19^{th}, since NO and NO_2 concentration were steadily below 5 ppb and 15 ppb (Figure B.2), and lead to a formation rate of 0.009 ppb $HONO_{sec}$/ (h (ppb NO_2)), consistently with the rate of (0.012±0.005) found by Alicke et al. (2002) in Milan by DOAS.

3.4. Nitric acid, nitrates and ammonia

Nitric acid is formed by reaction of $OH^{\cdot}$ with NO_2 leading to HNO_3 characteristic pattern featured by a single afternoon peak, when hydroxyl radicals are abundant. Nitric acid formation is expected to be controlled by the availability of $OH^{\cdot}$ rather than by NO_2, since HNO_3 diurnal pattern exhibits no difference between weekdays and Sundays, contrarily to NO_2, whose peak is above 12 ppb on weekdays and ∼5 ppb on Sundays.

Atmospheric particle nitrate is expected to be formed by two main pathways, either through reaction of HNO_3 with NH_3 or through absorption of $N_2O_{5(g)}$ (Lammel and Cape, 1996; Finlayson-Pitts and Pitts, 2000): the former reaction is homogeneous, the latter is heterogeneous and occurring only

at slow rates and at nighttime, since N_2O_5 and NO_3^- photolyse very rapidly (see Appendix A). The heterogeneous pathway is expected to form significant amount of aerosol nitrate: Alexander et al. (2009) estimated a similar contribution by the two pathways on an annual basis in Italy, while Michalski et al. (2003) estimated the heterogeneous pathway to contribute up to 50% to total summer nitrate in La Jolla (Southern California).

Diurnal pattern of nitrate shows an increase since 0200 to 1000 CEST during weekdays, whereas on Sundays exhibits steady concentration at mornings and an increase since 0900 to 1400 CEST. Afternoon patterns do not differ both in shape and levels between weekdays and Sundays. Two methods were used to investigate partitioning of ammonium nitrate with its precursors at thermodynamic equilibrium: ISORROPIA 2.1 (Fountoukis and Nenes, 2007) simulation model (forward mode and thermodynamically stable state conditions) and dissociation constants for reaction A.2 of ammonium nitrate aerosol assuming a single-component aerosol (see Appendix B for details and calculations). Both methods show how patterns of atmospheric nitrate and theoretical partitioning do not fully match (Figure S4), differently to other continental climate sites in summer (e.g. Melpitz, Germany (Poulain et al., 2011)), suggesting that condensation/evaporation processes do not exclusively control aerosol nitrate.

At nighttime N_2O_5 is expected to be partly responsible of the nitrate increase, also suggested by the slower formation rate compared to the one required by the thermodynamic equilibrium of the homogeneous reaction ac-

cording to ISORROPIA (not shown). The nitrate increase after sunrise is possibly kept up by homogeneous reaction A.2, triggered by the rapid formation of nitric acid from NO_2 rush hour emissions: since there is no evidence of nitric acid rise until 0900–1000, possibly this early morning HNO_3 is rapidly converted to nitrate. On Sundays nitrate increases from 0900–1000, i.e. most likely through the diurnal homogeneous reaction: the lower NO_2 levels over the weekend (Saturday and Sunday) lead to a smaller production of early morning HNO_3 and nighttime N_2O_5. Nitrate decreases during afternoons due to temperature increase and the shift of ammonium nitrate equilibrium to the gas-phase. Occasional morning increase in nitrate might be due also to re-entrainment of nitrate within the residual layer, which has been shown to provide a significant contribution to ground level concentration in Milan in summer (Curci et al., 2015).

Diurnal pattern for ammonia shows a steady profile. This is due to several reasons: total $NH_3 + NH_4^+$ is mainly in gasphase ammonia, therefore the particulate phase is not significantly affecting NH_3 concentration. Variability in aerosol nitrate diurnal pattern is almost negligible compared to ammonia levels, therefore no significant amount of ammonia is expected to be released in the afternoon when ammonium nitrate equilibrium moves towards gas-phase. Besides, in the afternoon HNO_3 increases, leading to ammonium nitrate formation partly compensating the dissociation of ammonium nitrate. Sulphate shows quite constant concentration and no significant change in NH_3 is expected from ammonium sulphate. Finally NH_3 emissions might

be slightly larger during daytime, but compensated by dilution from the enhanced boundary layer.

CBPF for nitrate shows how peak concentration of this compound is associated to very low wind speeds, i.e. is formed locally and concentrations increase due to the low dispersion conditions. On the contrary, median to moderate nitrate concentrations are associated to S or SSE winds, i.e. winds associated to moderate–large ammonia content. CBPF for ammonia indicates that larger observed levels are associated to distant sources at S, SSE, E and W of Milan, most likely emissions from agricultural activities in the Po valley surrounding the city. The existence of farther sources of ammonia were investigated also by BSMs (see Figure S5), which confirm emissions within the Po valley as main responsible for ammonia levels in Milan. This is consistent with 2010 emission inventories, ascribing 97% of all ammonia emissions to agricultural activities, and the remainder to traffic and wastewater treatment (Bigi and Ghermandi, under review).

During the campaign, significant pollution episodes occurred, both for particulate nitrate (June 8^{th}–9^{th}) and ammonia (June 27^{th}–28^{th}). The former occurred during a 48–hours period of relatively low temperature featured by a blocked atmosphere and an elevated inversion (Figure S6), the latter occurred during a rapid transport of ammonia originated in the Po valley (Figure S7).

3.5. Hydrochloric acid

Known anthropogenic sources of HCl are coal combustion (Lightowlers and Cape, 1988), biomass burning and waste incineration (Kaneyasu et al., 1999), whereas main natural source of HCl is sea-salt (Eldering et al., 1991). Few measurements of atmospheric HCl mixing ratios are reported in the literature and the data here presented are the first published measurements in Milan, to authors knowledge. Mean HCl level during the campaign resulted in 0.19 ppb. In summer 1999 Bari et al. (2003) observed 0.32 ppb and 0.28 ppb of HCl in two areas within New York City and attributed it to sea-salt. Eldering et al. (1991) observed HCl mixing ratios up to 3 ppb in Southern California in summer 1986 and demonstrated its formation by sea-salt chloride depletion by attack of HNO_3. Kaneyasu et al. (1999) showed the contribution of waste incineration to both atmospheric HCl and aerosol chloride during winter 1991 in the Japanese Kanto Plain, where chloride ranged between $10\,\mu g\,m^{-3}$ and over $70\,\mu g\,m^{-3}$. The study by Kaneyasu et al. (1999) showed how HCl emissions combined with NH_3 to $NH_4Cl_{(p)}$, which finally dissociate to gaseous HCl and NH_3 at daytime with warmer atmospheric temperatures.

Observed HCl in Milan exhibits no weekly pattern, but a clear diurnal pattern identically repeated throughout the week and best correlated to atmospheric temperature (see Figure B.1). This outcome was confirmed by a bivariate polar plot analysis conditioning concentration on atmospheric temperature instead of wind speed, indicating that higher HCl values are associated to higher temperature and do not depend on wind direction (Fig-

ure B.3). Atmospheric temperature is higher in the afternoons, when a SW breeze is established, explaining why in Figure B.3 larger HCl is associated to SW winds. The presence of a significant distant source (e.g. sea) for HCl was checked by BSMs, which pointed to a near source, excluding long range transport (see Figure S8). Similarly, the analysis of sodium chloride balance, considering both aerosol and gas phase, resulted in a large excess in Chlorine. These outcomes suggest that HCl is originated by a chlorinated compound free to evaporate in the atmosphere from a non-point source, and sufficiently abundant to generate significant atmospheric HCl levels. Unfortunately available data are not sufficient to explain this excess in Chloride and further samplings are needed to unveil the origin of HCl.

3.6. Sulphur dioxide and sulphates

SO_2 concentration in Milan are similar to other European cities (see Henschel et al., 2013, for an European overview) and its diurnal pattern, along with that of sulphate, shows no distinctive features, besides slightly lower concentrations on Sundays. Few stationary sources of SO_2 have significant emissions and are sufficiently near Milan to directly impact the city: the largest is an industrial area including a refinery and a carbon black manufacture sited 40 km West of the sampling site and emitting altogether $\sim$6 900 $\mathrm{Mg\,yr^{-1}}$ of SO_2 (E1 in Figure B.4). Other significant SO_2 sources are: a refinery sited 50 km South-West of the sampling site, with an estimated SO_2 emission of 4 500 $\mathrm{Mg\,yr^{-1}}$ (E2 in Figure B.4) and a refinery sited

130 km ESE (annual SO_2 emission of 1 600 Mg) (E3 in Figure B.4).

CBPF, bivariate polar plots and trajectory statistical models were used to identify whether any of the above potential source is impacting the sampling site. CBPF analysis associates low SO_2 levels (0.0–0.5 ppb, i.e. below the 20th quantile) to Northerly winds (CBPF plots for SO_2 are in Figure S9). Moderate SO_2 concentrations (20th–70th quantile) are associated to a Southern source (possibly E1 and/or Genoa) and a Western source (possibly E2). Highest concentrations are associated to a source SW of the site, most likely E1. Consistently bivariate polar plot for SO_2 associates mean levels to W and SW winds (Figure B.5e).

Potential sources of long-range transported SO_2 identified by BSMs were nearby Venice (250 km E of Milan) and in the Ligurian Sea/Ligurian shore (Figure S10). At the former a large refinery and a power plant are present; at the latter SO_2 emissions are expected by ship traffic and by a power plant (E4 in Figure B.4) which is partly coal fired. Finally some contribution could occur by sources nearby Marseille (E5 in Figure B.4), where an overall SO_2 emissions in the order of 50 000 $\mathrm{Mg\,yr^{-1}}$ is expected.

Regarding sulphate, CBPF associates its lowest concentration to Northerly winds (see Figure S11), similarly to SO_2. Low sulphate concentration is associated to low Eastern winds, possibly aged emissions from Venice or E3. Median sulphate levels (SO_4^{2-} ranging between 4.1–5.4 $\mu\mathrm{g\,m^{-3}}$, i.e. between 40th-60th quantile) are associated to moderate SW winds, suggesting a distant origin, eventually E4. Peaks in sulphate are associated to low SW winds

and possibly originate from E1 emissions. Backtrajectories models for sulphate suggest possible sources similar to SO_2 (Figure S12): all three statistical models indicate a source in the Ligurian sea, most likely maritime traffic and E4, a source nearby Venice and possibly some contribution from the area of Marseille. BSMs results consider transport from closer sources, within 36 hours travel distance: SO_2 oxidation rate for coal-fired power plant plume in summer was estimated as $\sim 1\,\%\,h^{-1}$ (Richards et al., 1981). Therefore the presence of other (e.g. more distant) sources of sulphate impacting Milan is possible, although their identification would require backtrajectories longer than 36 hours, better if associated to a particle dispersion model in order to provide reliable results for a BSMs (Han et al., 2005, e.g.) and beyond the aims of this study.

3.7. Elemental, organic and black carbon

EC exhibits a typical diurnal pattern of primary pollutants on weekdays, with a peak at 0800 CEST and a minimum when atmospheric mixing is highest. OC diurnal pattern on weekdays is featured by a slight afternoon increase due to secondary aerosol formation. The diurnal pattern for OC/EC ratio during weekdays, an index of secondary organic carbon formation, shows a minimum during primary emissions and a maximum during intense photochemical activity. No EC and OC data are available for Sundays. Following the rationale of Cabada et al. (2004), the EC tracer method was used to estimate secondary-influenced and primary-dominated OC, OC_s and OC_p

respectively. Hours with lower photochemical activity were selected upon ozone levels: for each day the 25th quantile of Ozone was computed and only OC EC data during hours with Ozone below this threshold have been used to estimate the OC_p to EC regression. Some limitations apply to this simplistic rationale for the Po valley, where large levels of SOA are expected even at low ozone concentration. The primary-dominated OC to EC linear fit resulted in a slope of 1.7 and an intercept of 2.9 $\mu g\,m^{-3}$ (Figure B.6), similarly to the ratio of 1.7 found by Lonati et al. (2007) for summer 2002 and 2003 on daily $PM_{2.5}$ samples in Milan. The intercept most likely includes sampling artefacts, non-combustion OC emissions (e.g. biogenic), meatcooking operations and background OC. These coefficients were used to estimate secondary organic aerosol (SOA) concentration and finally CBPF was used to estimate potential transport. Results show how peak SOA values are associated to winds from the SW sector, i.e. to afternoon winds with maximum solar radiation and photochemical activity. Median concentration of SOA are associated to Easterly winds, most likely transported from OC emissions within the Po valley.

Absorption coefficient by MAAP is well correlated to EC, leading to an average mass absorption coefficient MAC $= 13.8 \pm 0.2\,m^2g^{-1}$, in fair agreement to previous studies on off-line quartz fibre filters sampled in Milan (Vecchi et al., 2012). MAC is fairly constant throughout the day, with a daytime $MAC_{day} = 13.5 \pm 0.3\,m^2g^{-1}$ and night-time $MAC_{night} = 13.9 \pm 0.3\,m^2g^{-1}$ (Figure S13), indicating the same EC source, most likely traffic.

BC_E and EC, along with nitric oxide, show similar bivariate polar plots indicating a nearby main source sited SSE, along the direction of the nearest major road (see Figure B.5b for BC_E). CBPF associates lower concentration in BC_E and EC to SW winds, because of the dipersion induced by the stronger SW afternoon winds.

4. Conclusions

The article presented the most recent and complete analysis of 1-hour resolution observations of gaseous pollutants and main chemical composition of $PM_{2.5}$ in Milan. Ozone and nitrogen oxides pattern are consistent with intense photochemical activity under strong solar radiation, heavy emission sources and recirculation of pollutants, along with re-entrainment from the residual layer. HONO mixing rations, compared to 1998, exhibited a decrease, consistently with the reduction in NO_2 atmospheric concentration, although with a similar formation rate. Particulate nitrate formed through two pathways, depending upon the meteorological conditions and air mass origin. Backtrajectories and pollution rose models attributed sulphur dioxide and sulphate in Milan to emission sources in the Po valley, in the Ligurian coast and Ligurian sea. Steady high levels of ammonia have been observed throughout the campaign, originated mostly by agricultural emissions within the whole Po valley. A distinct pattern was observed for hydrochloric acid: several potential sources were investigated and results hints to evaporation of a chlorinated compound, although further studies are needed to provide a

clear answer.

The atmospheric stability conditions enduring during the campaign allowed to investigate in details processing and ageing of several gas phase and aerosol pollutants. Overall variability has been checked by hierarchical cluster analysis, with a distance matrix based on Pearson's correlation coefficient (Bigi and Ghermandi, 2014) and grouping driven by a divisive algorithm (Kaufman and Rousseeuw, 1990). Results showed a strong correlation among most pollutants and a modest cluster structure, featured by two groups (Figure S14): the first group includes long range transported pollutants (e.g. SO_2, SO_4^{2-}) and compounds strongly correlated to radiation and temperature. The second group includes locally emitted and locally formed pollutants, e.g. BC and NO_3^-. Implications of these results for local air quality policies are several: a large metropolitan area, although sited in a confined valley and under long-lasting atmospheric stability, can have air quality significantly affected by long-range transported pollutants. Moreover concentration variability of locally emitted pollutants in this same metropolitan area relies on the variability of overall emissions within the valley, therefore more attention needs to be paid to wide emissions, e.g. organic aerosol and ammonia. Conventional air quality policies aim to decrease concentration of regulatory pollutants (e.g. NO_2): we showed how their outcome controls the variation of less frequently monitored pollutants (e.g. HONO), whose influence on local air quality and climate is large and neglected by policymakers. Po valley plume stretches towards several European regions

surrounding Italy on the East and South (Finardi et al., 2014), including large parts of the Mediterranean sea, contributing to acidification and eutrophication (Jalkanen et al., 2000; Im et al., 2013). Study outlooks include a source apportionment analysis and deeper investigation of carbonaceous aerosol and secondary organic formation events.

Appendix A. Nitrate formation pathways

Formation of nitrate through homogeneous reaction pathway

$$NO_2 + OH^{\cdot} \rightarrow HNO_3 \tag{A.1}$$

$$HNO_3 + NH_3 \leftrightarrow NH_4NO_{3(s,aq)} \tag{A.2}$$

Formation of nitrate through heterogeneous reaction pathway with nighttime formation of nitrate radical $NO_3^{\cdot}$, its reaction to dinitrogen pentoxide N_2O_5, the hydrolysis of N_2O_5 on surfaces releasing $HNO_{3(aq)}$ which is finally hydrolysed to nitrate, similarly to the reaction A.2.

$$NO_2 + O_3 \rightarrow NO_{3(g)}^{\cdot} + O_2 \tag{A.3}$$

$$NO_{3(g)}^{\cdot} + NO_{2(g)} \leftrightarrow N_2O_{5(g)} \tag{A.4}$$

$$N_2O_{5(g)} + H_2O_{(l)} \rightarrow 2HNO_{3(aq)} \tag{A.5}$$

$$HNO_{3(aq)} + NH_{3(g)} \leftrightarrow NH_{4(aq)}^{+} + NO_{3(aq)}^{-} \tag{A.6}$$

Appendix B. Calculation of equilibrium constants for ammonium nitrate

K_p and K_p^* are the dissociation constants for solid phase and aqueous ammonium nitrate respectively, estimated according to Mozurkewich (1993). K_{AN} is the equilibrium constant for reaction A.2, estimated according to Seinfeld and Pandis (2006) and Poulain et al. (2011).

Deliquescence relative humidity for ammonium nitrate (Seinfeld and Pandis, 2006):

$$\ln(\mathrm{DRH}) = \frac{723.7}{T} + 1.6954 \tag{B.1}$$

Dissociation constant K_p for solid ammonium nitrate formed through reaction A.2 (Mozurkewich, 1993):

$$\ln(K_p) = 118.87 - \frac{24084}{T} - 6.025 \ln(T) \tag{B.2}$$

Dissociation constant K_p^* for aqueous ammonium nitrate formed through reaction A.2 (Mozurkewich, 1993):

$$K_p^* = \left(P_1 - P_2(1-a_w) + P_3(1-a_w)^2\right) \cdot (1-a_w)^{1.75} \cdot K_p \tag{B.3}$$

with

$$\ln(P_1) = -135.94 + \frac{8763}{T} + 19.12 \ln(T) \tag{B.4}$$

$$\ln(P_2) = -122.65 + \frac{9969}{T} + 16.22 \ln(T) \tag{B.5}$$

$$\ln(P_1) = -182.61 + \frac{13875}{T} + 24.46\ln(T) \quad \text{(B.6)}$$

and water activity a_w approximated by RH expressed in the range 0–1. Equilibrium constant K_{AN} of ammonium nitrate at RH above that of deliquescence ammonium nitrate, in ppb^2 from Poulain et al. (2011).

$$K_{AN} = k(298)\exp\left\{a\left(\frac{298}{T} - 1\right) + b\left[1 + \ln\left(\frac{298}{T}\right) - \frac{298}{T}\right]\right\} \cdot 10^{-18} \quad \text{(B.7)}$$

with $k(298) = 3.35 \cdot 10^{-16}\,\text{atm}^{-2}$, $a = 75.11$, $b = -13.5$

Acknowledgements Thanks to Luca Lombroso for the description of the synoptic meteorological conditions.

Acker, K., Mller, D., Auel, R., Wieprecht, W., and Kala, D.: Concentrations of nitrous acid, nitric acid, nitrite and nitrate in the gas and aerosol phase at a site in the emission zone during ESCOMPTE 2001 experiment, Atmospheric Research, 74, 507 – 524, doi:10.1016/j.atmosres.2004.04.009, 2005.

AERA: OGC-WMS Server http://geomap.reteunitaria.piemonte.it/ws/aera/rp-01/aerawms/wms_aera_emissioni_tot?, last access: 2015-01-07, 2015.

Alexander, B., Hastings, M. G., Allman, D. J., Dachs, J., Thornton, J. A., and Kunasek, S. A.: Quantifying atmospheric nitrate formation pathways based on a global model of the oxygen isotopic composition (Δ^{17}O) of

628 atmospheric nitrate, Atmospheric Chemistry and Physics, 9, 5043–5056,
629 doi:10.5194/acp-9-5043-2009, 2009.

630 Alicke, B., Platt, U., and Stutz, J.: Impact of nitrous acid photolysis on the
631 total hydroxyl radical budget during the Limitation of Oxidant Produc-
632 tion/Pianura Padana Produzione di Ozono study in Milan, Journal of Geo-
633 physical Research: Atmospheres, 107, 8196, doi:10.1029/2000JD000075,
634 2002.

635 Bae, M.-S., Schauer, J. J., DeMinter, J. T., Turner, J. R., Smith, D., and
636 Cary, R. A.: Validation of a semi-continuous instrument for elemental
637 carbon and organic carbon using a thermal-optical method, Atmospheric
638 Environment, 38, 2885–2893, doi:10.1016/j.atmosenv.2004.02.027, 2004.

639 Baltensperger, U., Streit, N., Weingartner, E., Nyeki, S., Prévôt, A. S. H.,
640 Van Dingenen, R., Virkkula, A., Putaud, J.-P., Even, A., ten Brink, H.,
641 Blatter, A., Neftel, A., and Gäggeler, H. W.: Urban and rural aerosol
642 characterization of summer smog events during the PIPAPO field cam-
643 paign in Milan, Italy, Journal of Geophysical Research, D107, 8193, doi:
644 10.1029/2001JD001292, 2002.

645 Bari, A., Ferraro, V., Wilson, L. R., Luttinger, D., and Husain, L.: Mea-
646 surements of gaseous HONO, HNO3, SO2, HCl, NH3, particulate sulfate
647 and PM2.5 in New York, NY, Atmospheric Environment, 37, 2825–2835,
648 doi:10.1016/S1352-2310(03)00199-7, 2003.

649 Bernardoni, V., Vecchi, R., Valli, G., Piazzalunga, A., and Fermo,
650 P.: PM10 source apportionment in Milan (Italy) using time-resolved
651 data, Science of The Total Environment, 409, 4788 – 4795, doi:
652 10.1016/j.scitotenv.2011.07.048, 2011.

653 Bigi, A. and Ghermandi, G.: Long-term trend and variability of atmospheric
654 PM_{10} concentration in the Po Valley, Atmospheric Chemistry and Physics,
655 14, 4895–4907, doi:10.5194/acp-14-4895-2014, 2014.

656 Bigi, A. and Ghermandi, G.: Trends and variability of atmospheric $PM_{2.5}$
657 and $PM_{10-2.5}$ concentration in the Po Valley, Italy, Atmospheric Chemistry
658 and Physics Discussions, under review.

659 Bigi, A., Ghermandi, G., and Harrison, R. M.: Analysis of the air pollution
660 climate at a background site in the Po valley, Journal of Environmental
661 Monitoring, 14, 552–563, doi:10.1039/c1em10728c, 2012.

662 Cabada, J., Pandis, S., Subramanian, R., Robinson, A., Polidori, A., and
663 Turpin, B.: Estimating the Secondary Organic Aerosol Contribution to
664 $PM_{2.5}$ Using the EC Tracer Method, Aerosol Science and Technology, 38,
665 140–155, doi:10.1080/02786820390229084, 2004.

666 Carslaw, D. and Ropkins, K.: openair – an R package for air quality data
667 analysis, Environmental Modelling & Software, 27–28, 52–61, 2012.

668 Cavalli, F., Viana, M., Yttri, K. E., Genberg, J., and Putaud, J.-P.: Toward
669 a standardised thermal-optical protocol for measuring atmospheric organic

and elemental carbon: the EUSAAR protocol, Atmospheric Measurement Techniques, 3, 79–89, doi:10.5194/amt-3-79-2010, 2010.

Cleveland, W. S., Graedel, T. E., Kleiner, B., and Warner, J. L.: Sunday and Workday Variations in Photochemical Air Pollutants in New Jersey and New York, Science, 186, 1037–1038, doi:10.1126/science.186.4168.1037, 1974.

Curci, G., Ferrero, L., Tuccella, P., Barnaba, F., Angelini, F., Bolzacchini, E., Carbone, C., Denier van der Gon, H. A. C., Facchini, M. C., Gobbi, G. P., Kuenen, J. P. P., Landi, T. C., Perrino, C., Perrone, M. G., Sangiorgi, G., and Stocchi, P.: How much is particulate matter near the ground influenced by upper-level processes within and above the PBL? A summertime case study in Milan (Italy) evidences the distinctive role of nitrate, Atmospheric Chemistry and Physics, 15, 2629–2649, doi:10.5194/acp-15-2629-2015, 2015.

D'Alessandro, A., Lucarelli, F., Mand, P., Marcazzan, G., Nava, S., Prati, P., Valli, G., Vecchi, R., and Zucchiatti, A.: Hourly elemental composition and sources identification of fine and coarse PM10 particulate matter in four Italian towns, Journal of Aerosol Science, 34, 243–259, doi:10.1016/S0021-8502(02)00172-6, 2003.

D'Alessandro, A., Lucarelli, F., Marcazzan, G., Nava, S., Prati, P., Valli, G., Vecchi, R., and Zucchiatti, A.: A summertime investigation on urban

691 PM fine and coarse fractions using hourly elemental concentration data
692 series, Nuovo Cimento della Societa Italiana di Fisica C, 27, 17–28, doi:
693 10.1393/ncc/i2003-10015-7, 2004.

694 Draxler, R. and Rolph, G.: HYSPLIT (HYbrid Single-Particle Lagrangian
695 Integrated Trajectory), Model access via NOAA ARL READY Website
696 (http://www.arl.noaa.gov/HYSPLIT.php), 2013.

697 Eldering, A., Solomon, P. A., Salmon, L. G., Fall, T., and Cass, G. R.:
698 Hydrochloric acid: A regional perspective on concentrations and formation
699 in the atmosphere of Southern California, Atmospheric Environment. Part
700 A. General Topics, 25, 2091 – 2102, doi:10.1016/0960-1686(91)90086-M,
701 1991.

702 Febo, A., Perrino, C., and Allegrini, I.: Measurement of nitrous acid in
703 Milan, Italy, by DOAS and diffusion denuders, Atmospheric Environment,
704 30, 3599–3609, doi:10.1016/1352-2310(96)00069-6, 1996.

705 Finardi, S., Silibello, C., DAllura, A., and Radice, P.: Analysis
706 of pollutants exchange between the Po Valley and the surround-
707 ing European region, Urban Climate, 10, Part 4, 682 – 702, doi:
708 http://dx.doi.org/10.1016/j.uclim.2014.02.002, 2014.

709 Finlayson-Pitts, B. J. and Pitts, J. N.: Chemistry of the upper and lower
710 atmosphere, Academic Press, San Diego, USA, 2000.

711 Fleming, Z. L., Monks, P. S., and Manning, A. J.: Review: Un-
712 tangling the influence of air-mass history in interpreting observed at-
713 mospheric composition, Atmospheric Research, 104105, 1 – 39, doi:
714 10.1016/j.atmosres.2011.09.009, 2012.

715 Fountoukis, C. and Nenes, A.: ISORROPIA II: a computationally efficient
716 thermodynamic equilibrium model for K^+–Ca^{2+}–Mg^{2+}–NH_4^+–Na^+–SO_4^{2-}–
717 NO_3^-–Cl^-–H_2O aerosols, Atmospheric Chemistry and Physics, 7, 4639–
718 4659, doi:10.5194/acp-7-4639-2007, 2007.

719 Gutzwiller, L., Arens, F., Baltensperger, U., Gggeler, H. W., and Ammann,
720 M.: Significance of Semivolatile Diesel Exhaust Organics for Secondary
721 HONO Formation, Environmental Science & Technology, 36, 677–682, doi:
722 10.1021/es015673b, 2002.

723 Han, Y., , Holsen, T., Hopke, P., and Yi, S.: Comparison between Back-
724 Trajectory Based Modeling and Lagrangian Backward Dispersion Mod-
725 eling for Locating Sources of Reactive Gaseous Mercury, Environmental
726 Science & Technology, 39, 1715–1723, doi:10.1021/es0498540, 2005.

727 Henschel, S., Querol, X., Atkinson, R., Pandolfi, M., Zeka, A., Tertre,
728 A. L., Analitis, A., Katsouyanni, K., Chanel, O., Pascal, M., Bouland,
729 C., Haluza, D., Medina, S., and Goodman, P. G.: Ambient air SO2 pat-
730 terns in 6 European cities, Atmospheric Environment, 79, 236–247, doi:
731 10.1016/j.atmosenv.2013.06.008, 2013.

Im, U., Christodoulaki, S., Violaki, K., Zarmpas, P., Kocak, M., Daskalakis, N., Mihalopoulos, N., and Kanakidou, M.: Atmospheric deposition of nitrogen and sulfur over southern Europe with focus on the Mediterranean and the Black Sea, Atmospheric Environment, 81, 660–670, doi: 10.1016/j.atmosenv.2013.09.048, 2013.

INEMAR: www.inemar.eu, last access: 2015-01-07, 2015.

Jalkanen, L., Mkinen, A., Hsnen, E., and Juhanoja, J.: The effect of large anthropogenic particulate emissions on atmospheric aerosols, deposition and bioindicators in the eastern Gulf of Finland region, Science of the Total Environment, 262, 123–136, doi:10.1016/S0048-9697(00)00602-1, 2000.

Jarvis, A., Reuter, H. I., Nelson, A., and Guevara, E.: Hole-filled seamless SRTM data V4, Tech. rep., International Centre for Tropical Agriculture (CIAT), URL `http://srtm.csi.cgiar.org`, 2008.

Jiménez, P., Parra, R., Gassó, S., and Baldasano, J. M.: Modeling the ozone weekend effect in very complex terrains: a case study in the Northeastern Iberian Peninsula, Atmospheric Environment, 39, 429 – 444, doi: http://dx.doi.org/10.1016/j.atmosenv.2004.09.065, 2005.

Jung, J., Kim, Y. J., Lee, K. Y., Kawamura, K., Hu, M., and Kondo, Y.: The effects of accumulated refractory particles and the peak inert mode temperature on semi-continuous organic carbon and elemental carbon mea-

surements during the CAREBeijing 2006 campaign, Atmospheric Environment, 45, 7192 – 7200, doi:10.1016/j.atmosenv.2011.09.003, 2011.

Kalberer, M., Ammann, M., Arens, F., Gggeler, H. W., and Baltensperger, U.: Heterogeneous formation of nitrous acid (HONO) on soot aerosol particles, Journal of Geophysical Research: Atmospheres, 104, 13 825–13 832, doi:10.1029/1999JD900141, 1999.

Kaneyasu, N., Yoshikado, H., Mizuno, T., Sakamoto, K., and Soufuku, M.: Chemical forms and sources of extremely high nitrate and chloride in winter aerosol pollution in the Kanto Plain of Japan, Atmospheric Environment, 33, 1745 – 1756, doi:10.1016/S1352-2310(98)00396-3, 1999.

Kaufman, L. and Rousseeuw, P. J.: Finding groups in data : an introduction to cluster analysis, Wiley, New York, 1990.

Kleffmann, J.: Daytime Sources of Nitrous Acid (HONO) in the Atmospheric Boundary Layer, ChemPhysChem, 8, 1137–1144, doi: 10.1002/cphc.200700016, 2007.

Kleffmann, J., Lrzer, J., Wiesen, P., Kern, C., Trick, S., Volkamer, R., Rodenas, M., and Wirtz, K.: Intercomparison of the DOAS and LOPAP techniques for the detection of nitrous acid (HONO), Atmospheric Environment, 40, 3640 – 3652, doi:10.1016/j.atmosenv.2006.03.027, 2006.

Kurtenbach, R., Becker, K., Gomes, J., Kleffmann, J., Lrzer, J., Spittler, M., Wiesen, P., Ackermann, R., Geyer, A., and Platt, U.: Investiga-

tions of emissions and heterogeneous formation of HONO in a road traffic tunnel, Atmospheric Environment, 35, 3385 – 3394, doi:10.1016/S1352-2310(01)00138-8, 2001.

Lammel, G. and Cape, J. N.: Nitrous acid and nitrite in the atmosphere, Chem. Soc. Rev., 25, 361–369, doi:10.1039/CS9962500361, 1996.

Lightowlers, P. and Cape, J.: Sources and fate of atmospheric HCl in the U.K. and Western Europe, Atmospheric Environment (1967), 22, 7 – 15, doi:10.1016/0004-6981(88)90294-6, 1988.

Lonati, G., Ozgen, S., and Giugliano, M.: Primary and secondary carbonaceous species in PM2.5 samples in Milan (Italy), Atmospheric Environment, 41, 4599 – 4610, doi:10.1016/j.atmosenv.2007.03.046, 2007.

Marcazzan, G., Caprioli, E., Valli, G., and Vecchi, R.: Temporal variation of ^{212}Pb concentration in outdoor air of Milan and a comparison with ^{214}Bi, Journal of Environmental Radioactivity, 65, 77–90, doi:10.1016/S0265-931X(02)00089-9, 2003.

Markovic, M. Z., VandenBoer, T. C., and Murphy, J. G.: Characterization and optimization of an online system for the simultaneous measurement of atmospheric water-soluble constituents in the gas and particle phases, Journal of Environmental Monitoring, 14, 1872–1884, doi:10.1039/C2EM00004K, 2012.

793 Michalski, G., Scott, Z., Kabiling, M., and Thiemens, M. H.: First measure-
794 ments and modeling of Δ^{17}O in atmospheric nitrate, Geophysical Research
795 Letters, 30, doi:10.1029/2003GL017015, 2003.

796 Michoud, V., Colomb, A., Borbon, A., Miet, K., Beekmann, M., Camre-
797 don, M., Aumont, B., Perrier, S., Zapf, P., Siour, G., Ait-Helal, W., Afif,
798 C., Kukui, A., Furger, M., Dupont, J. C., Haeffelin, M., and Doussin,
799 J. F.: Study of the unknown HONO daytime source at a European sub-
800 urban site during the MEGAPOLI summer and winter field campaigns,
801 Atmospheric Chemistry and Physics, 14, 2805–2822, doi:10.5194/acp-14-
802 2805-2014, 2014.

803 Mozurkewich, M.: The dissociation constant of ammonium nitrate and
804 its dependence on temperature, relative humidity and particle size, At-
805 mospheric Environment. Part A. General Topics, 27, 261 – 270, doi:
806 http://dx.doi.org/10.1016/0960-1686(93)90356-4, 1993.

807 Neftel, A., Spirig, C., Prévôt, A. S. H., Furger, M., Stutz, J., Vogel, B., and
808 Hjorth, J.: Sensitivity of photooxidant production in the Milan Basin: An
809 overview of results from a EUROTRAC-2 Limitation of Oxidant Produc-
810 tion field experiment, Journal of Geophysical Research: Atmospheres, 107,
811 8188, doi:10.1029/2001JD001263, 2002.

812 Penkett, S., Jones, B., Brich, K., and Eggleton, A.: The importance of
813 atmospheric ozone and hydrogen peroxide in oxidising sulphur dioxide in

814 cloud and rainwater, Atmospheric Environment (1967), 13, 123 – 137, doi:
815 10.1016/0004-6981(79)90251-8, 1979.

816 Perrone, M., Larsen, B., Ferrero, L., Sangiorgi, G., Gennaro, G. D., Udisti,
817 R., Zangrando, R., Gambaro, A., and Bolzacchini, E.: Sources of high
818 PM2.5 concentrations in Milan, Northern Italy: Molecular marker data
819 and CMB modelling, Science of The Total Environment, 414, 343 – 355,
820 doi:10.1016/j.scitotenv.2011.11.026, 2012.

821 Petzold, A., Kramer, H., and Schönlinner, M.: Continuous measurement
822 of atmospheric black carbon using a multi-angle absorption photometer,
823 Environmental Science and Pollution Research, 4, 78–82, 2002.

824 Pollack, I., Ryerson, T., Trainer, M., Parrish, D., Andrews, A., Atlas, E.,
825 Blake, D., Brown, S., Commane, R., Daube, B., De Gouw, J., Dub, W.,
826 Flynn, J., Frost, G., Gilman, J., Grossberg, N., Holloway, J., Kofler, J.,
827 Kort, E., Kuster, W., Lang, P., Lefer, B., Lueb, R., Neuman, J., Nowak,
828 J., Novelli, P., Peischl, J., Perring, A., Roberts, J., Santoni, G., Schwarz,
829 J., Spackman, J., Wagner, N., Warneke, C., Washenfelder, R., Wofsy,
830 S., and Xiang, B.: Airborne and ground-based observations of a weekend
831 effect in ozone, precursors, and oxidation products in the California South
832 Coast Air Basin, Journal of Geophysical Research: Atmospheres, 117, doi:
833 10.1029/2011JD016772, 2012.

834 Poulain, L., Spindler, G., Birmili, W., Plass-Dülmer, C., Wiedensohler, A.,
835 and Herrmann, H.: Seasonal and diurnal variations of particulate nitrate

836 and organic matter at the IfT research station Melpitz, Atmospheric Chem-
837 istry and Physics, 11, 12 579–12 599, doi:10.5194/acp-11-12579-2011, 2011.

838 Putaud, J.-P., Van Dingenen, R., and Raes, F.: Submicron aerosol mass bal-
839 ance at urban and semirural sites in the Milan area (Italy), Journal of Geo-
840 physical Research: Atmospheres, 107, 8198, doi:10.1029/2000JD000111,
841 2002.

842 Putaud, J.-P., Van Dingenen, R., Alastuey, A., Bauer, H., Birmili, W., Cyrys,
843 J., Flentje, H., Fuzzi, S., Gehrig, R., Hansson, H. C., Harrison, R. M., Her-
844 rmann, H., Hitzenberger, R., Hglin, C., Jones, A. M., Kasper-Giebl, A.,
845 Kiss, G., Kousa, A., Kuhlbusch, T. A. J., Lschau, G., Maenhaut, W.,
846 Molnar, A., Moreno, T., Pekkanen, J., Perrino, C., Pitz, M., Puxbaum,
847 H., Querol, X., Rodriguez, S., Salma, I., Schwarz, J., Smolik, J., Schnei-
848 der, J., Spindler, G., ten Brink, H., Tursic, J., Viana, M., Wiedensohler,
849 A., and Raes, F.: A European aerosol phenomenology - 3: Physical and
850 chemical characteristics of particulate matter from 60 rural, urban, and
851 kerbside sites across Europe, Atmospheric Environment, 44, 1308 – 1320,
852 doi:10.1016/j.atmosenv.2009.12.011, 2010.

853 R Core Team: R: A Language and Environment for Statistical Computing,
854 R Foundation for Statistical Computing, Vienna, Austria, 2013.

855 Ravishankara, A. R.: Heterogeneous and Multiphase Chemistry in the Tropo-
856 sphere, Science, 276, 1058–1065, doi:10.1126/science.276.5315.1058, 1997.

857 Richards, L., Anderson, J., Blumenthal, D., Brandt, A., Mcdonald, J., Wa-
858 ters, N., Macias, E., and Bhardwaja, P.: Plumes and Visibility Measure-
859 ments and Model Components The chemistry, aerosol physics, and optical
860 properties of a western coal-fired power plant plume, Atmospheric Environ-
861 ment, 15, 2111 – 2134, doi:http://dx.doi.org/10.1016/0004-6981(81)90245-
862 6, 1981.

863 Scheifinger, H. and Kaiser, A.: Validation of trajectory statis-
864 tical methods, Atmospheric Environment, 41, 8846–8856, doi:
865 10.1016/j.atmosenv.2007.08.034, 2007.

866 Seinfeld, J. H. and Pandis, S. N.: Atmospheric Chemistry and Physics, Wiley,
867 2nd edn., 2006.

868 Spindler, G., Hesper, J., Brggemann, E., Dubois, R., Mller, T., and Her-
869 rmann, H.: Wet annular denuder measurements of nitrous acid: laboratory
870 study of the artefact reaction of NO_2 with S(IV) in aqueous solution and
871 comparison with field measurements, Atmospheric Environment, 37, 2643
872 – 2662, doi:http://dx.doi.org/10.1016/S1352-2310(03)00209-7, 2003.

873 Stutz, J., Alicke, B., and Neftel, A.: Nitrous acid formation in the urban
874 atmosphere: Gradient measurements of NO_2 and HONO over grass in
875 Milan, Italy, Journal of Geophysical Research: Atmospheres, 107, doi:
876 10.1029/2001JD000390, 2002.

877 Tonse, S., Brown, N., Harley, R., and Jin, L.: A process-analysis based study

878 of the ozone weekend effect, Atmospheric Environment, 42, 7728–7736, doi:
879 10.1016/j.atmosenv.2008.05.061, 2008.

880 Uria-Tellaetxe, I. and Carslaw, D. C.: Conditional bivariate probability func-
881 tion for source identification, Environmental Modelling & Software, 59, 1
882 – 9, doi:http://dx.doi.org/10.1016/j.envsoft.2014.05.002, 2014.

883 Vecchi, R. and Valli, G.: Ozone assessment in the southern part of the Alps,
884 Atmospheric Environment, 33, 97–109, doi:10.1016/S1352-2310(98)00133-
885 2, 1999.

886 Vecchi, R., Valli, G., Fermo, P., D'Alessandro, A., Piazzalunga,
887 A., and Bernardoni, V.: Organic and inorganic sampling arte-
888 facts assessment, Atmospheric Environment, 43, 1713 – 1720, doi:
889 10.1016/j.atmosenv.2008.12.016, 2009.

890 Vecchi, R., Valli, G., Bernardoni, V., Paganelli, C., and Piazzalunga, A.:
891 Insights on BC determination on quartz-fibre and PTFE filters: results of
892 two field experiments in Milan (Italy), in: Proceedings of the European
893 Aerosol Conference 2012, edited by Alados-Arboledas, L. and Olmo Reyes,
894 F. J., AWG08S1P17, European Aerosol Assembly, Granada, Spain, 2012.

895 Wang, Y., Hu, B., Ji, D., Liu, Z., Tang, G., Xin, J., Zhang, H., Song, T.,
896 Wang, L., Gao, W., Wang, X., and Wang, Y.: Ozone weekend effects in the
897 Beijing-Tianjin-Hebei metropolitan area, China, Atmospheric Chemistry
898 and Physics, 14, 2419–2429, doi:10.5194/acp-14-2419-2014, 2014.

Wood, S.: Generalized Addittive Models: an introduction with R, Chapman & Hall/CRC, Boca Raton, USA, 2006.

World Health Organization: Air quality guidelines. Global update 2005. Particulate matter, ozone, nitrogen dioxide and sulfur dioxide, World Health Organization, Regional office for Europe, Copenhagen, Denmark, 2006.

Zhang, J. and Trivikrama Rao, S.: The Role of Vertical Mixing in the Temporal Evolution of Ground-Level Ozone Concentrations, Journal of Applied Meteorology, 38, 1674–1691, doi:10.1175/1520-0450(1999)038<1674:TROVMI>2.0.CO;2, 1999.

Ziemba, L. D., Dibb, J. E., Griffin, R. J., Anderson, C. H., Whitlow, S. I., Lefer, B. L., Rappenglck, B., and Flynn, J.: Heterogeneous conversion of nitric acid to nitrous acid on the surface of primary organic aerosol in an urban atmosphere, Atmospheric Environment, 44, 4081 – 4089, doi:10.1016/j.atmosenv.2008.12.024, 2010.

Table B.1: Statistical values of gas, particles and meteorological parameters during the whole campaign. Note: for global radiation the range of maximum diurnal is indicated; for precipitation the total rainfall and the maxium intensity are indicated.

Parameter	Mean $\pm\sigma$	Median
Nitric oxide (NO), ppb	4.58 ± 2.66	4.00
Nitrogen dioxide (NO_2), ppb	6.41 ± 6.46	4.18
Nitrogen oxides as NO_2 (NO_x), ppb	10.99 ± 8.10	8.00
Ozone (O_3), ppb	41.73 ± 19.73	41.10
Organic carbon (OC), $\mu g\,m^{-3}$	6.16 ± 4.53	4.42
Elemental carbon (EC), $\mu g\,m^{-3}$	0.70 ± 0.61	0.62
Equivalent black carbon (BC_E), $\mu g\,m^{-3}$	1.59 ± 1.16	1.25
Hydrochloric acid (HCl), ppb	0.19 ± 0.20	0.12
Ammonia (NH_3), ppb	14.40 ± 5.25	13.18
Nitrous acid (HONO), ppb	0.55 ± 0.34	0.49
Nitric acid (HNO_3), ppb	0.71 ± 0.51	0.60
Sulphur dioxide (SO_2), ppb	0.92 ± 0.50	0.79
Calcium ion (Ca^{2+}), $\mu g\,m^{-3}$	0.27 ± 0.21	0.20
Chloride ion (Cl^-), $\mu g\,m^{-3}$	0.10 ± 0.21	0.10
Potassium ion (K^+), $\mu g\,m^{-3}$	0.08 ± 0.18	0.10
Magnesium ion (Mg^{2+}), $\mu g\,m^{-3}$	0.04 ± 0.10	0.00
Sodium ion (Na^+), $\mu g\,m^{-3}$	0.67 ± 0.79	0.30
Ammonium ion (NH_4^+), $\mu g\,m^{-3}$	5.63 ± 3.40	5.00
Nitrite ion (NO_2^-), $\mu g\,m^{-3}$	1.01 ± 0.58	0.90
Nitrate ion (NO_3^-), $\mu g\,m^{-3}$	2.72 ± 3.15	1.80
Sulphate ion (SO_4^{2-}), $\mu g\,m^{-3}$	4.82 ± 2.22	4.60
Atmospheric pressure (p), hPa	996.6 ± 3.9	996.3
Atmospheric temperature (T), C	26.0 ± 4.5	25.8
Global radiation (GR), $W\,m^{-2}$	396.20 – 909.67	
Precipitation (r), mm – $mm\,h^{-1}$	134.8 – 29.4	
Radon (Rn), $Bq\,m^{-3}$	6.1 ± 4.0	4.8
Relative humidity (RH), %	51.9 ± 16.0	50.4
Wind speed (W), $m\,s^{-1}$	1.2 ± 0.9	1.1

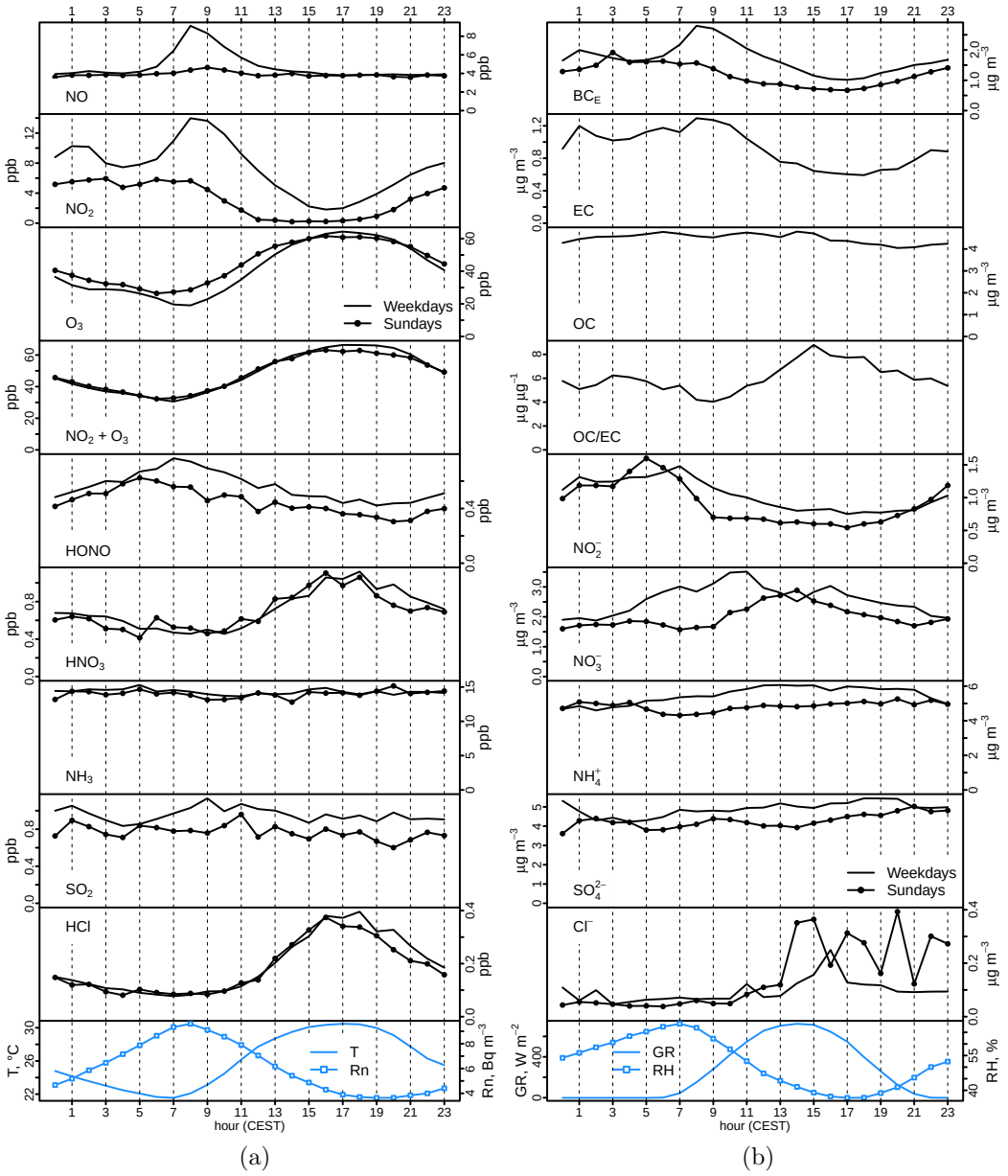

Figure B.1: Diurnal pattern for weekdays and Sundays for several gas phase (panel a) and particle phase (panel b) pollutants. Diurnal pattern of few meteorological variables and parameters are also included: temperature (T), Radon concentration (Rn), global radiation (GR) and relative humidity (RH).

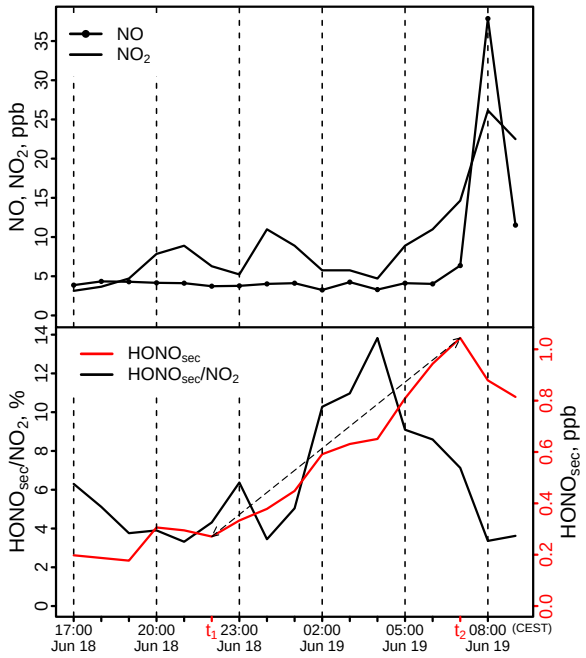

Figure B.2: Formation of $HONO_{sec}$ during the night between June 18^{th}–19^{th} 2012. The arrows indicate the data used to calculate first-order formation rate.

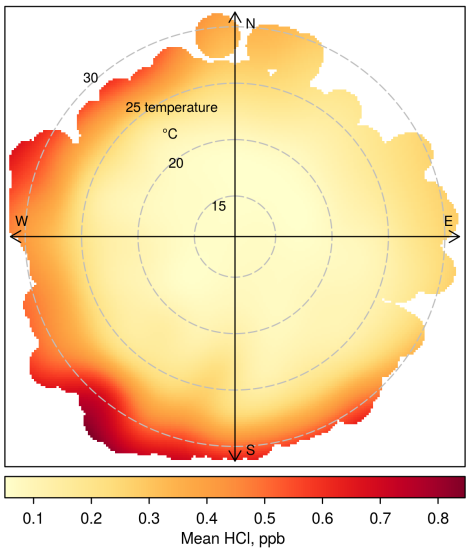

Figure B.3: Bivariate polar plots for hydrochloric acid with atmospheric temperature (°C) as radial scale.

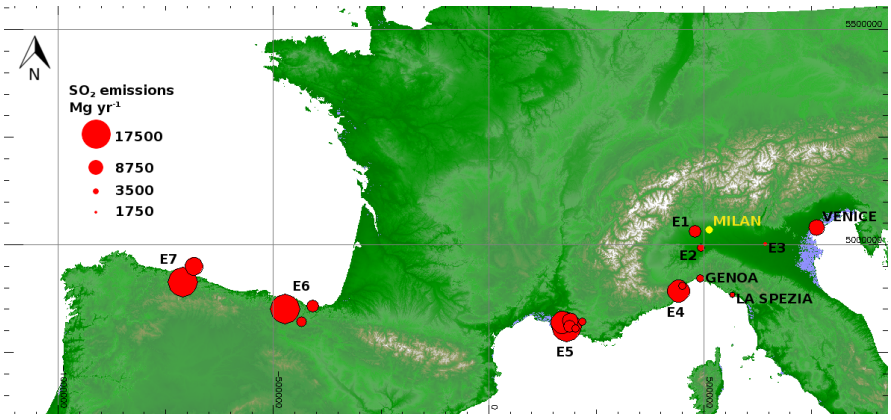

Figure B.4: Annual SO_2 emissions from point sources which potentially impacted on sulphur dioxide and sulphate ambient concentration in Milan in summer 2012 (DEM provided by Jarvis et al. (2008)).

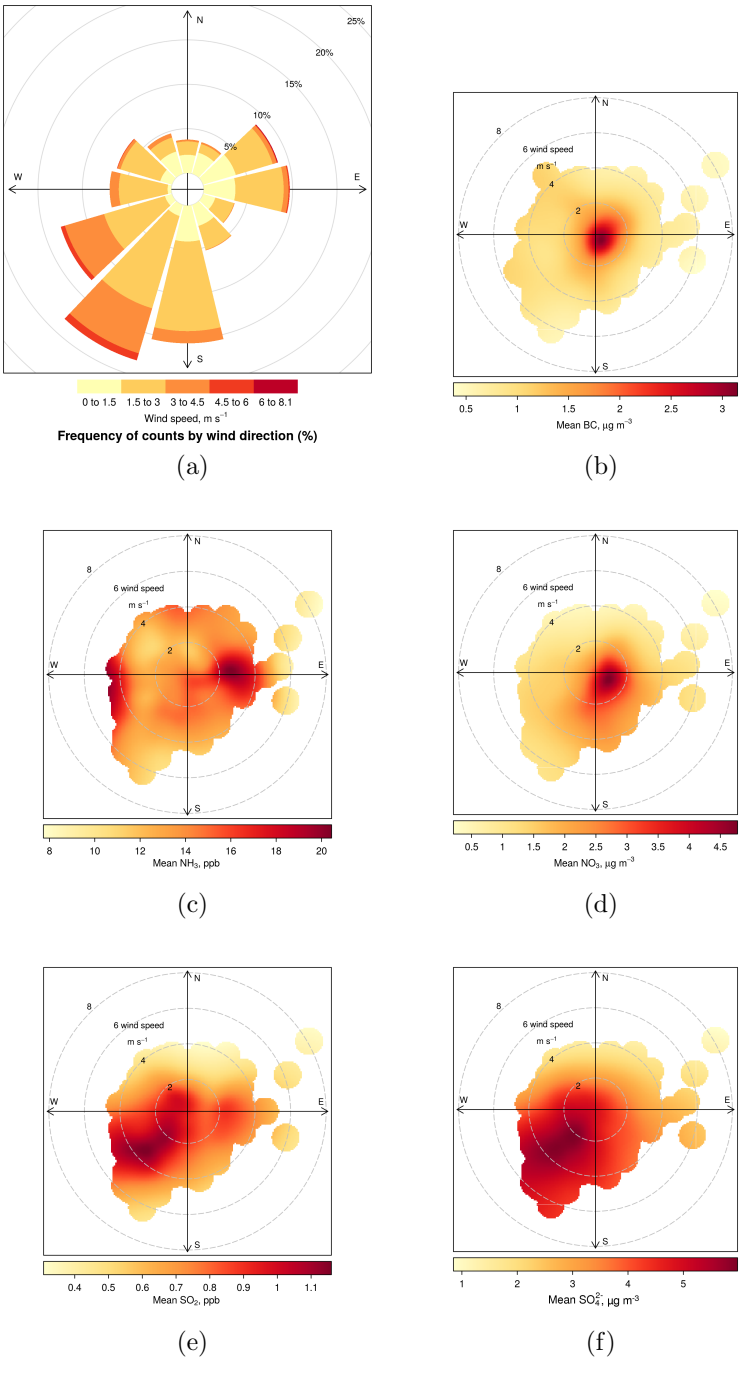

Figure B.5: Wind rose and bivariate polar plot of BC_E, NH_3, NO_3^-, SO_2 and SO_4^{2-}; colour codes correspond to concentration for each direction; circles correspond to wind speed.

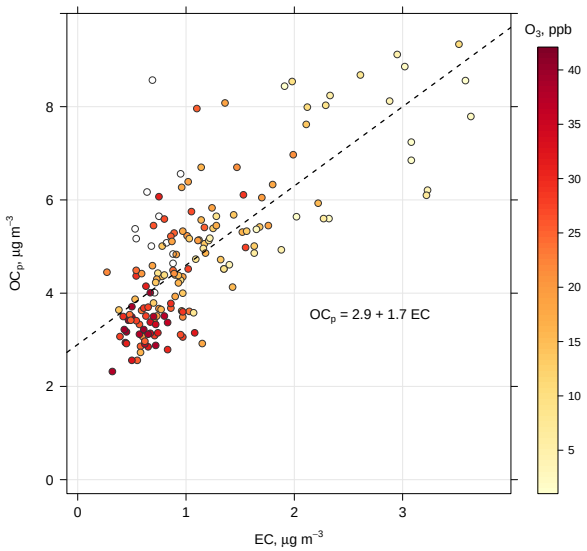

Figure B.6: Scatter plot of primary-dominated OC (OC_p) vs EC data, colour-coded according to O_3 levels. Dashed line represents the linear regression model fit for the estimate of the OC_p/EC ratio.

Supplementary Material

Click here to download Supplementary Interactive Plot Data (CSV): supplementary_material_rev.pdf

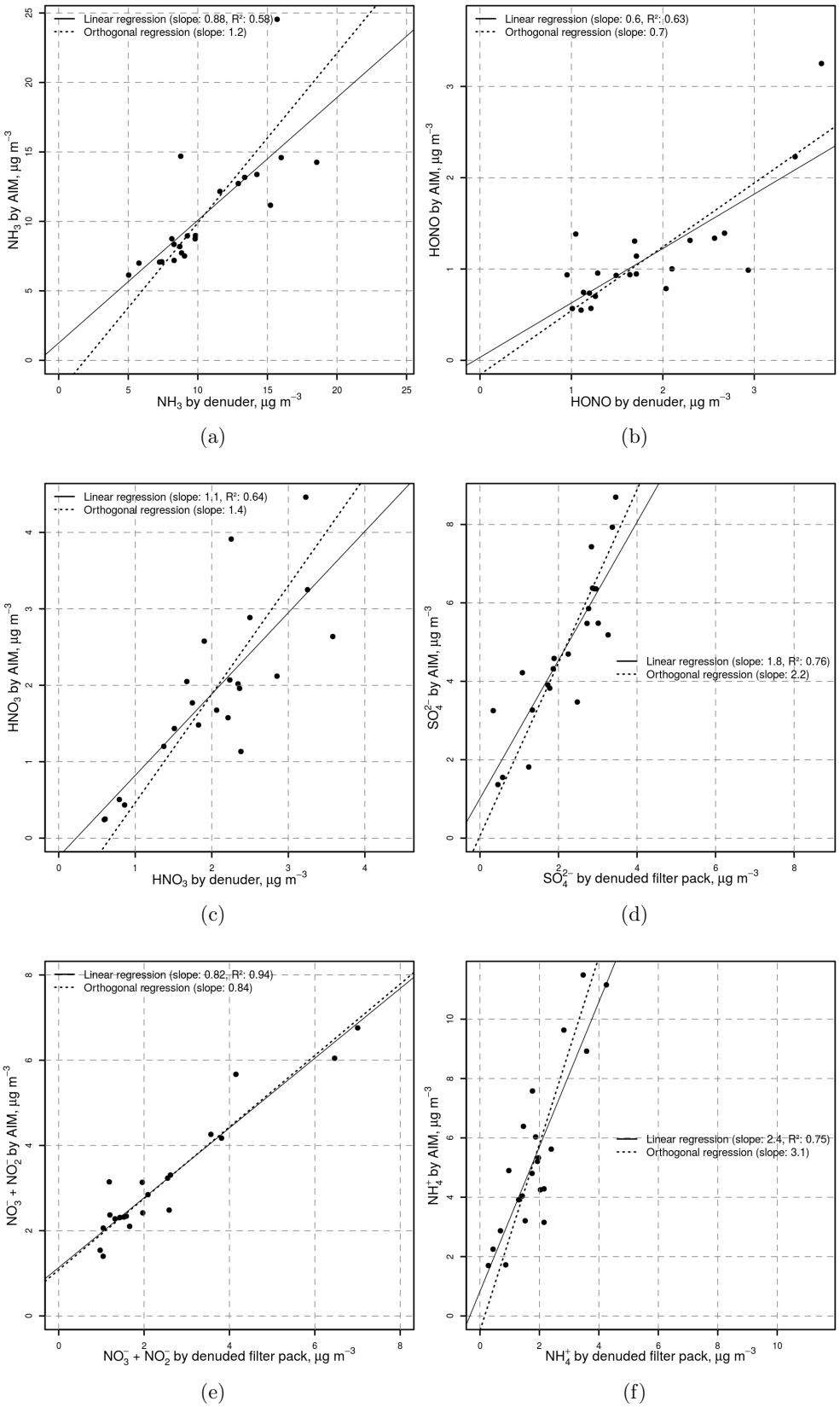

Figure S1: Scatterplot and regression models between on-line and off-line data by AIM data and denuded filter pack respectively.

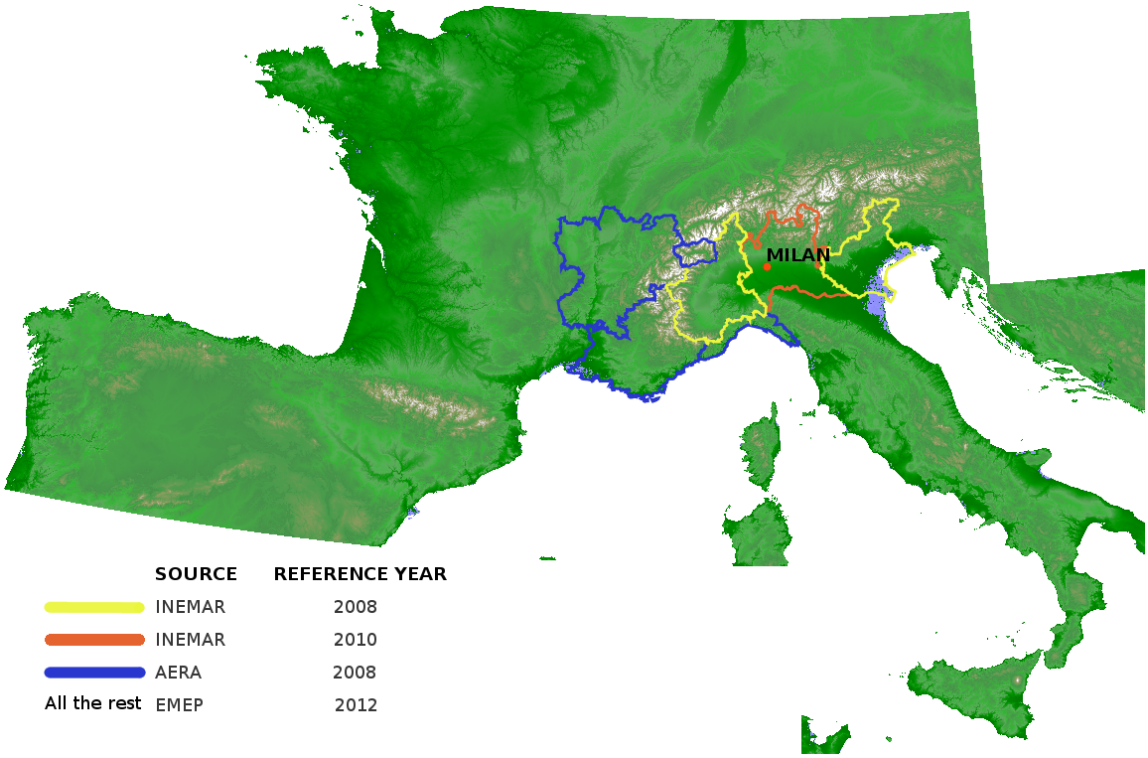

Figure S2: Graphical match between region and the emission inventory used.

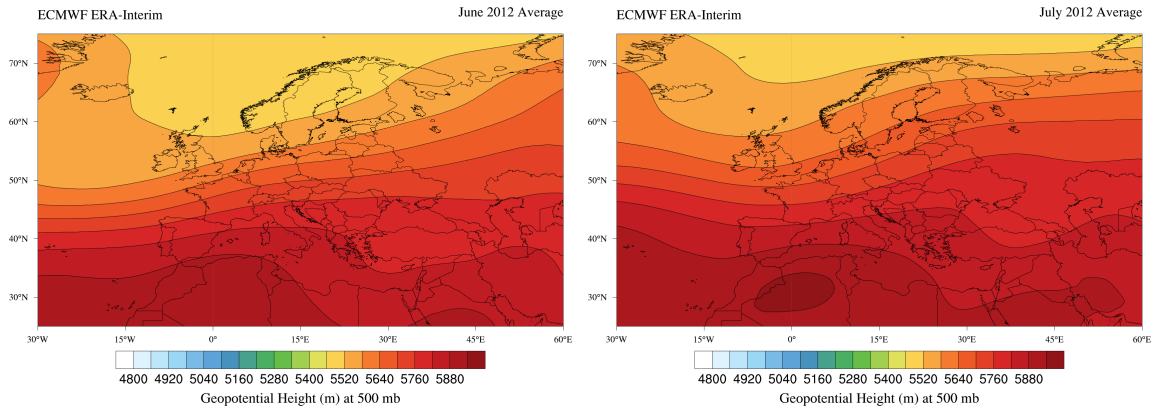

(a)

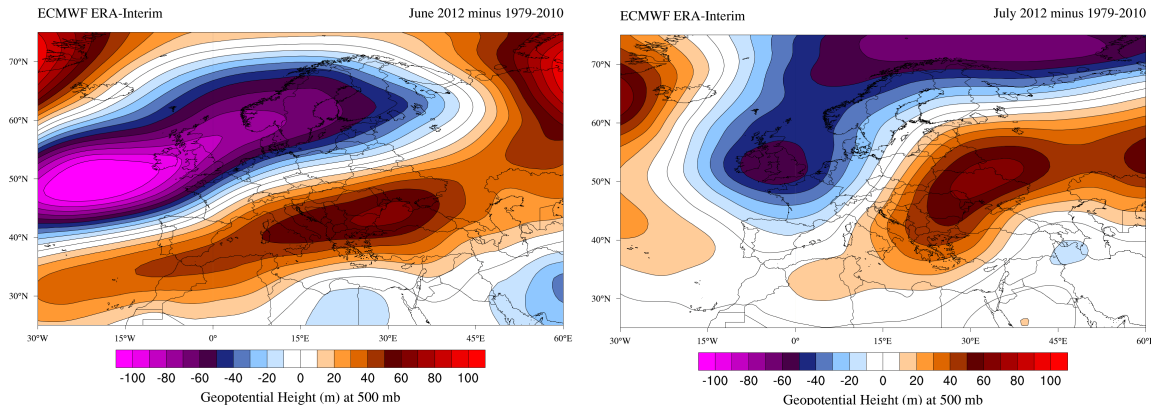

(b)

Figure S3: Mean monthly 500 hPa geopotential height (a) and anomaly (b) by ERA-Interim reanalysis. ERA-Interim — ECWMF obtained using Climate Reanalyzer (http://cci-reanalyzer.org), Climate Change Institute, University of Maine, USA.

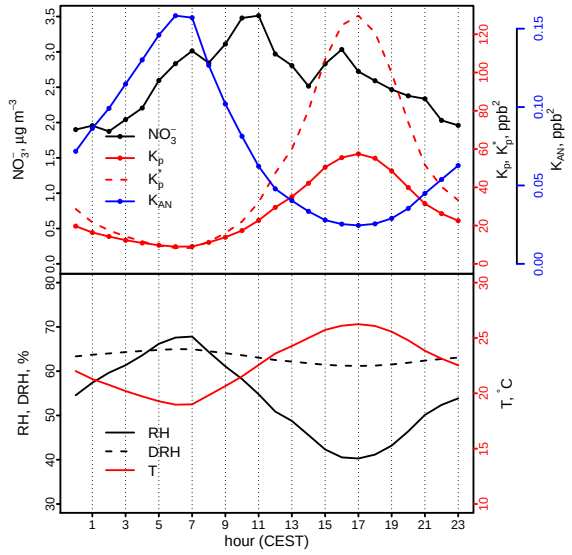

(a)

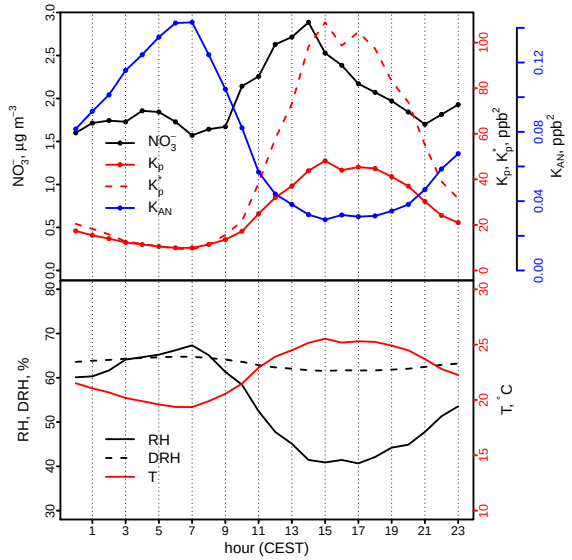

(b)

Figure S4: Diurnal pattern on weekdays (a) and Sundays (b) for nitrate and ammonium nitrate thermodynamic properties.

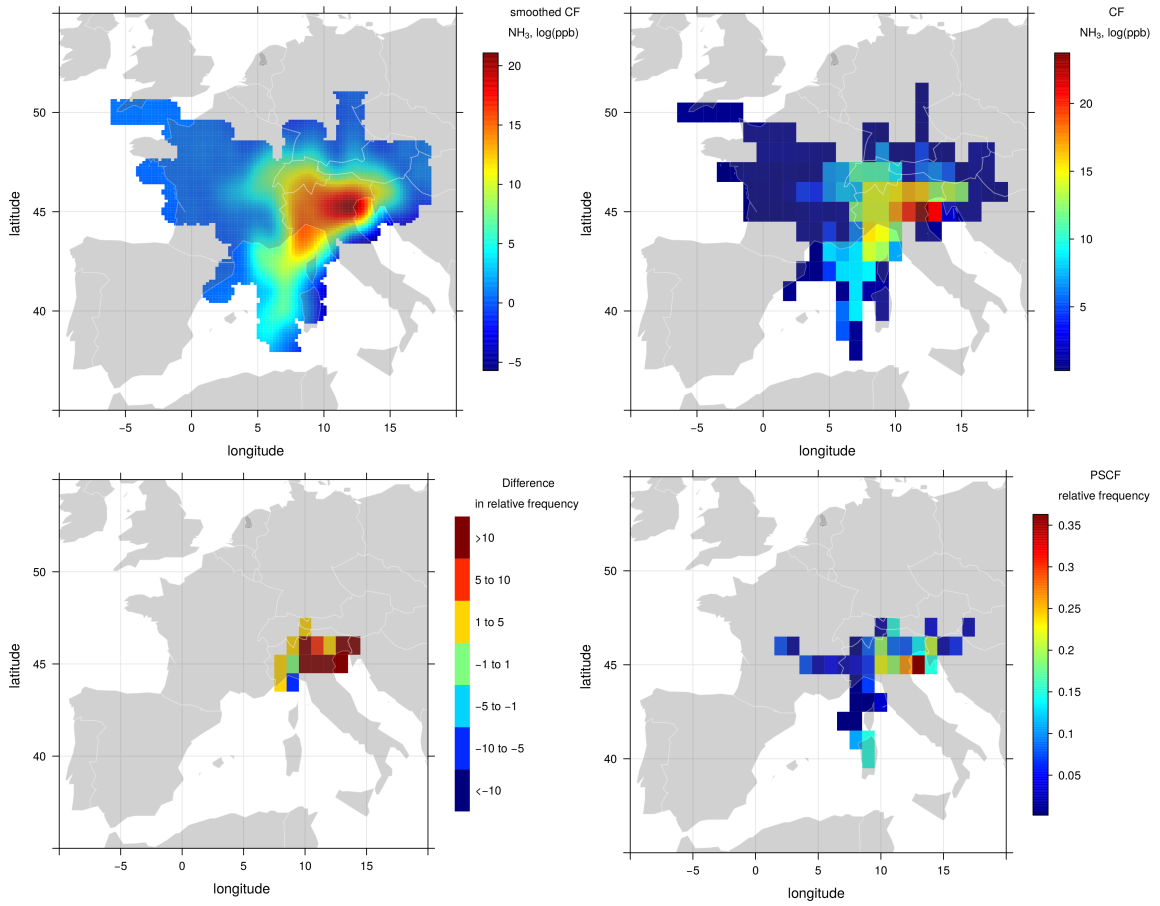

Figure S5: Graphical output of backtrajectory statistical models applied to NH_3 concentration observed in Milan.

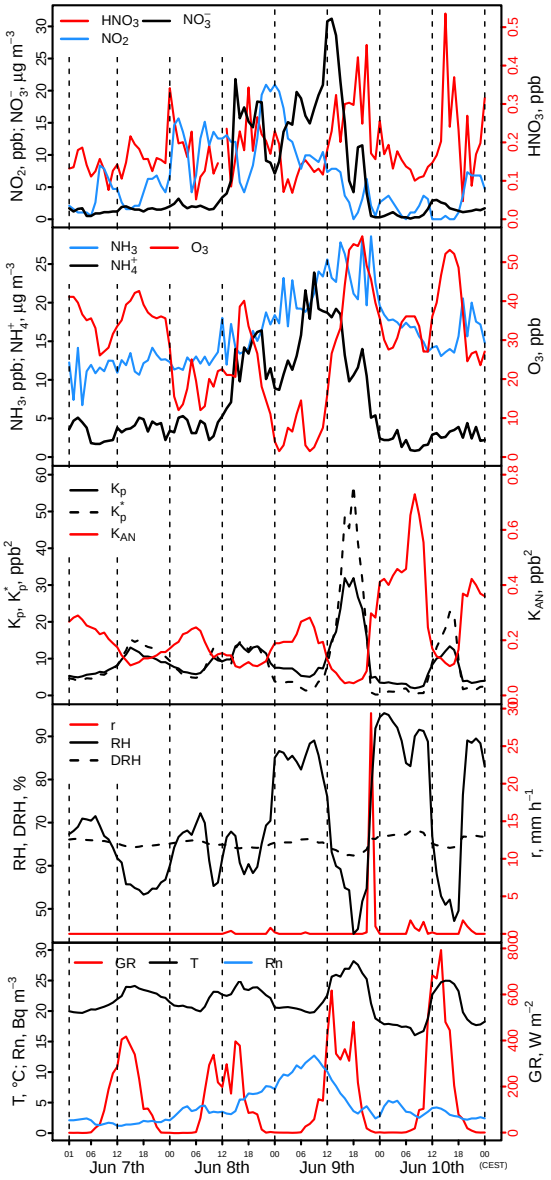

Figure S6: Overview of the nitrate peak event during June 8$^{\text{th}}$–9$^{\text{th}}$ 2012

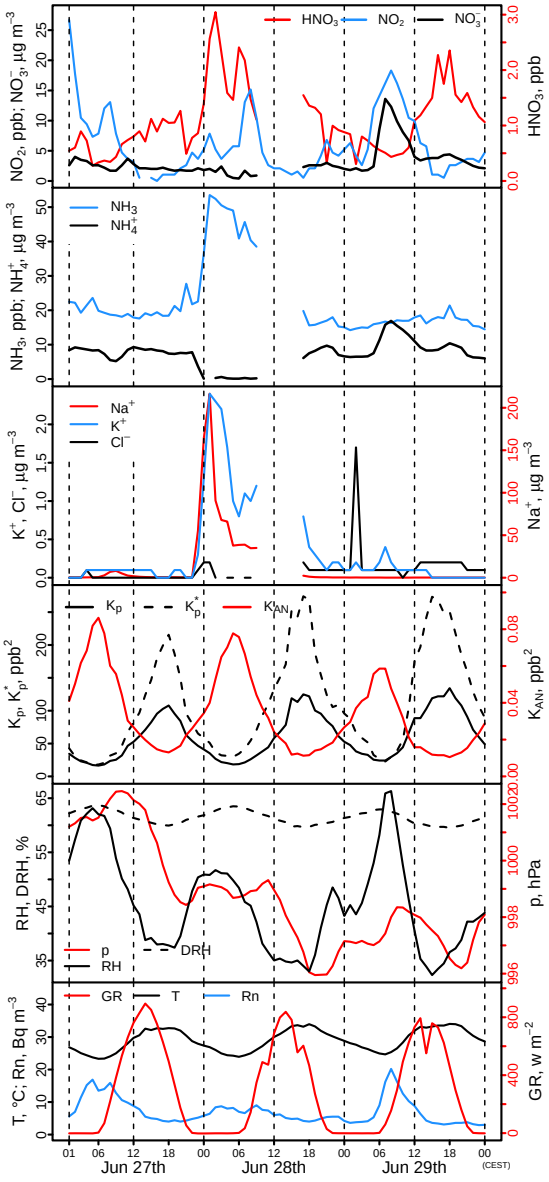

Figure S7: Overview of the ammonia peak event during June 27$^{\text{th}}$–29$^{\text{th}}$ 2012

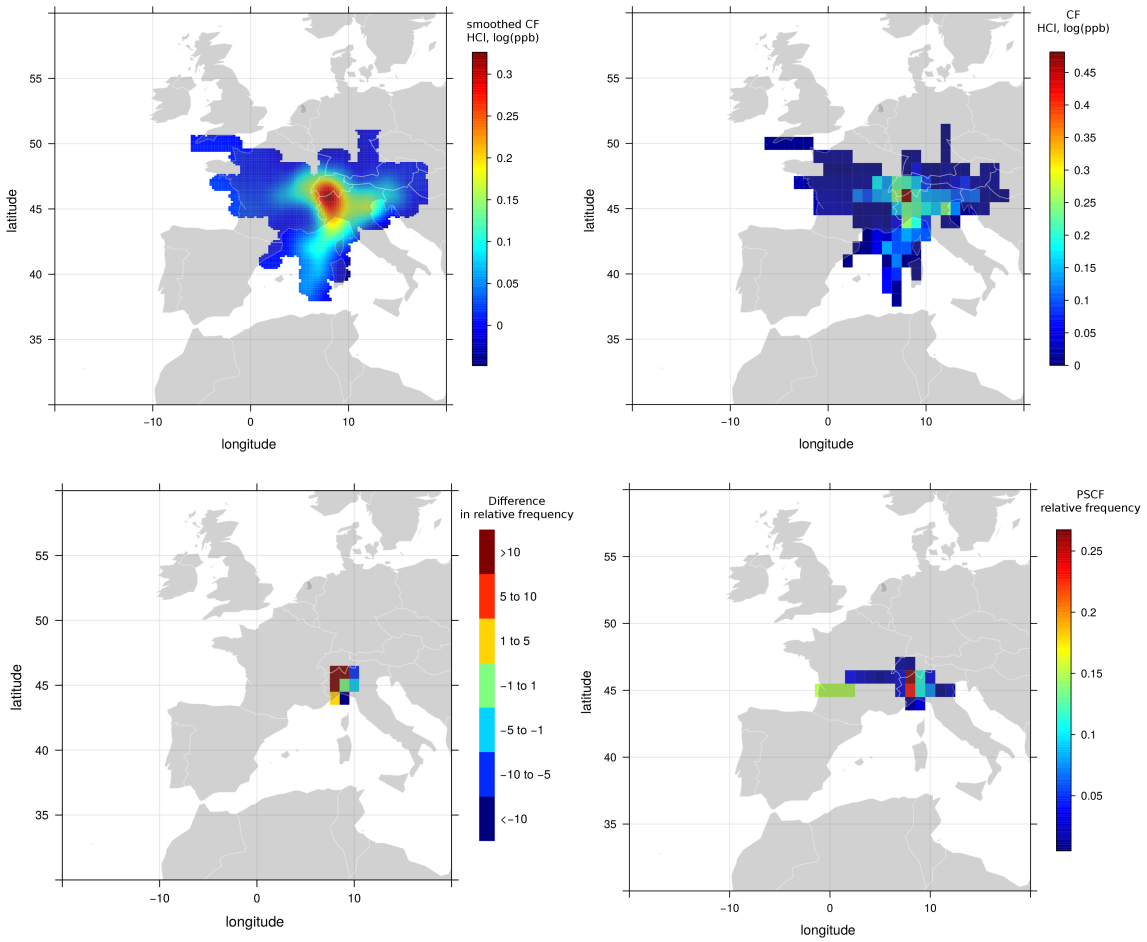

Figure S8: Graphical output of backtrajectory statistical models applied to HCl concentration observed in Milan.

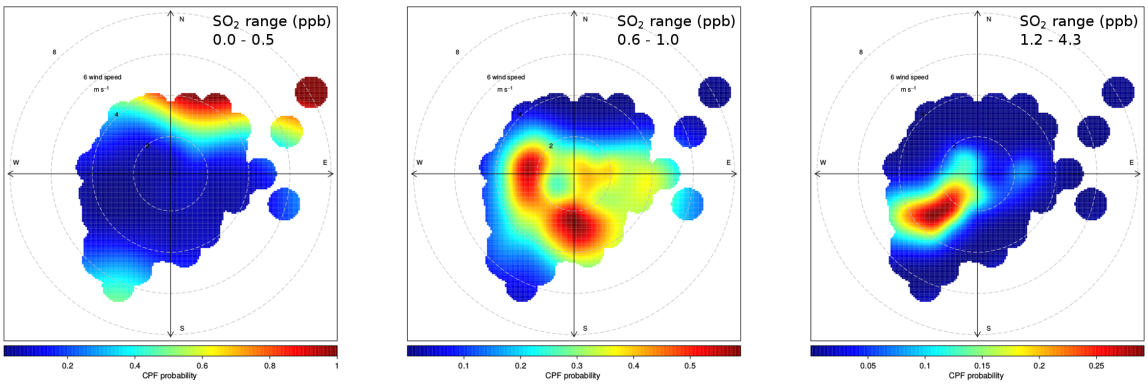

Figure S9: CBPF for SO_2 concentration observed in Milan.

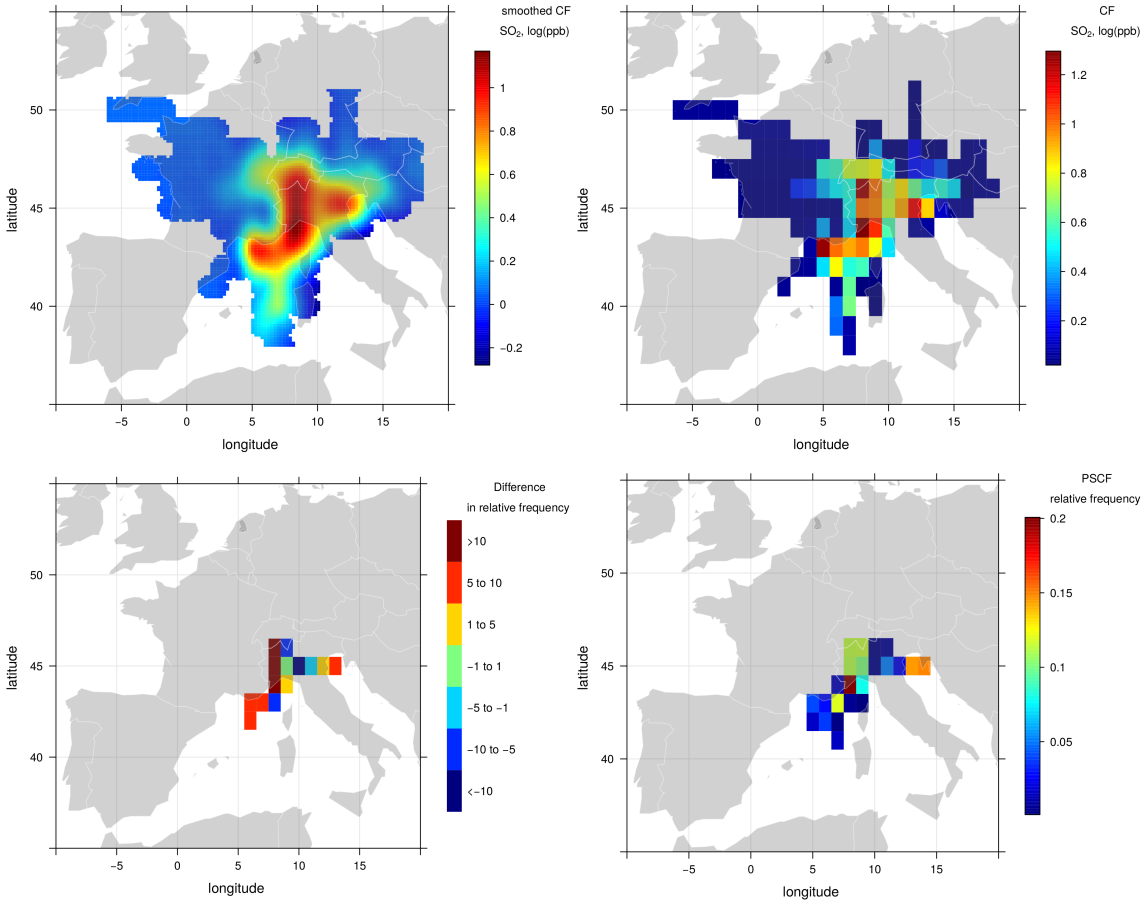

Figure S10: Graphical output of backtrajectory statistical models applied to SO_2 concentration observed in Milan.

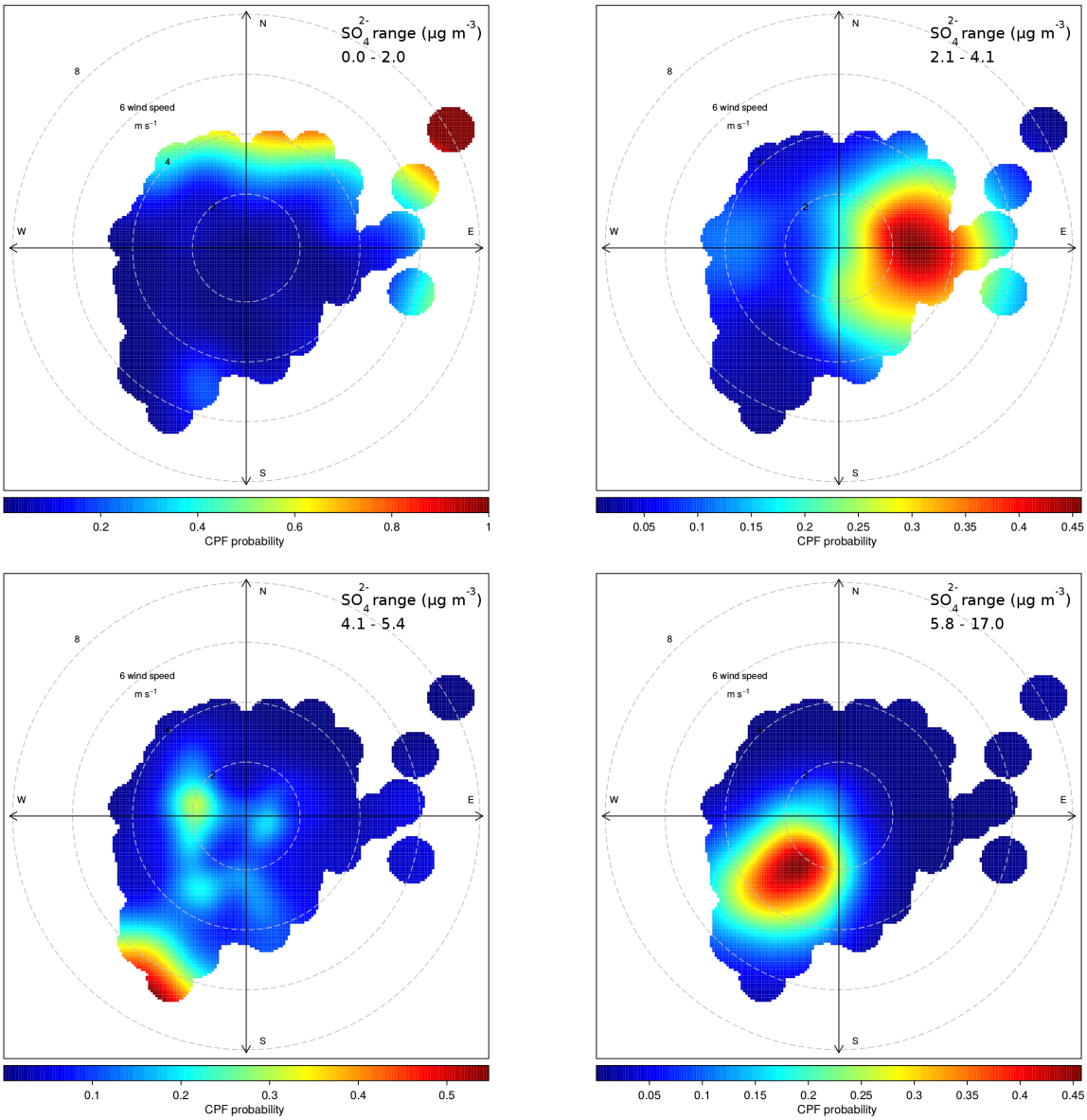

Figure S11: CBPF for SO_4^{2-} concentration observed in Milan.

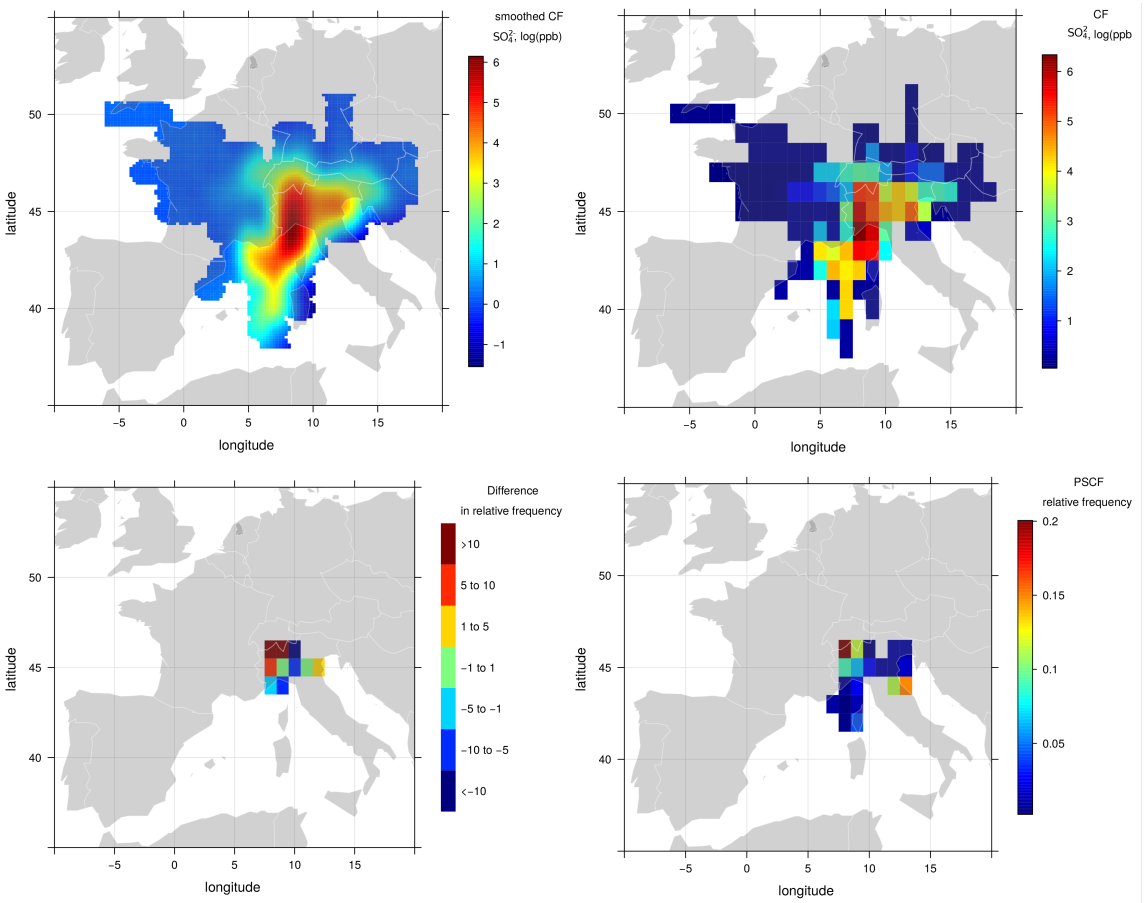

Figure S12: Graphical output of backtrajectory statistical models applied to SO_4^{2-} concentration observed in Milan.

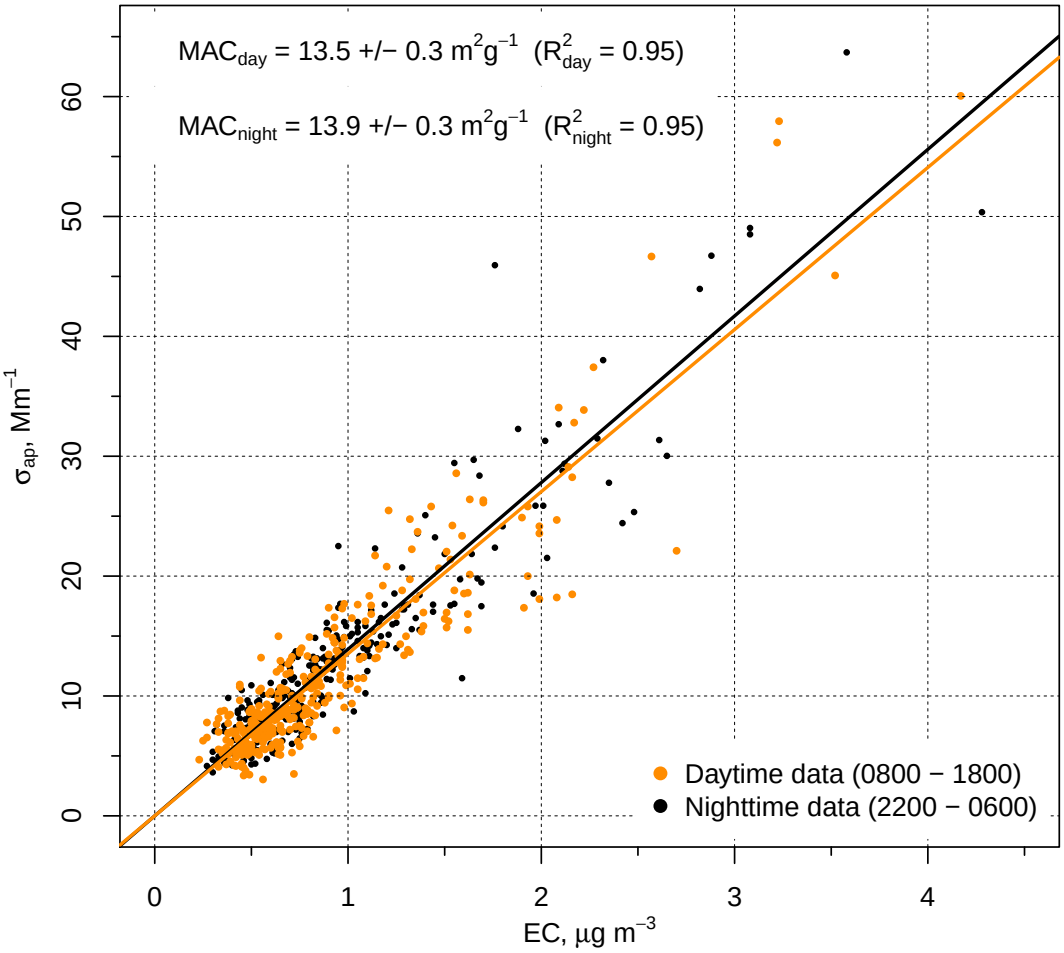

Figure S13: Scatterplot and linear model fit between absorption coefficient by MAAP (σ_{ap}) and Elemental Carbon concentration by ECOC field analyzer (EC) .

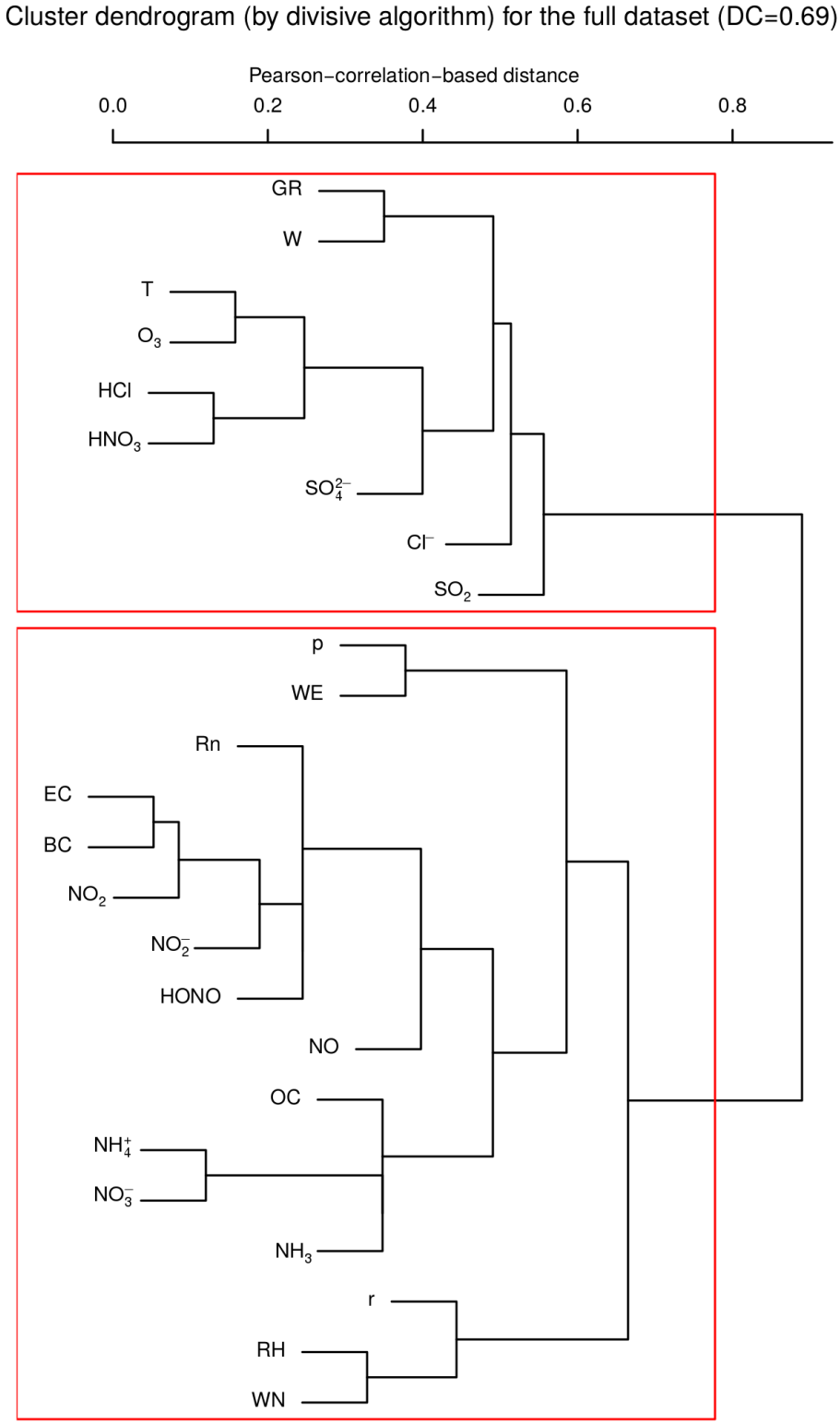

Figure S14: Results of cluster analysis on the complete dataset data using a Pearson-correlation-based distance. Coloured boxes indicate clusters; lookup table for abbreviations can be found in table B.1. WN and WE are the Northern and Eastern component of wind vector, DC is the Divisive Coefficient.